Coherent photoproduction of two neutral pseudoscalar mesons on light nuclei

Mikhail Egorov*

Federal State Unitary Enterprise "Russian Federal Nuclear Center" Academician E.I. Zababakhin All-Russian Research Institute of Technical Physics, Snezhinsk, Chelyabinsk Region, Russia

(Received 8 February 2020; accepted 9 June 2020; published 24 June 2020)

Coherent photoproduction of $\pi^0\pi^0$ and $\pi^0\eta$ on nuclei with $A \leqslant 7$ is systematically studied in the energy region from the threshold to the laboratory photon energy $E_\gamma = 2$ GeV. The amplitude of photoproduction on nuclei is derived in the impulse approximation taking account of certain processes responsible for the meson-nucleus final-state interaction. For the first time, the unified microscopic approach is used to calculate effects such as rescattering of the $\pi N \to \pi N$ and $\pi N \to \eta N$ pions from spectator nucleons, photoproduction of $\pi^{+/-}\pi^0\pi^0$ and $\pi^{+/-}\pi^0\eta$, and the follow-on absorption of $\pi^{+/-}$ by spectator nucleons, as well as three-body π-NN and η-NN interaction among effects being responsible for the meson-nucleus final-state interaction. Direct calculation shows total cross sections of $\pi^0\pi^0$ and $\pi^0\eta$ photoproduction to be strongly dependent both on the target nucleus isospin, and the target nucleus model.

DOI: 10.1103/PhysRevC.101.065205

I. INTRODUCTION

The key objective of quantum chromodynamics, including its lattice versions, is to describe spectra of the baryon ground and excited states in modes with the partially and completely broken chiral symmetry [1]. Though advancements in chromodynamics theories are quite obvious, color confinement and role of the excited gluonic field in the formation of baryon spectra still remain unclear. Great success in creating baryon spectra was achieved by constituent quark models [2–4], as well as AdS/QCD theory [correspondence between the conformal supersymmetric SU(4) gauge field theory and supergravitation in the $AdS_5 \times S_5$ space] [5,6]. Partial recovery of chiral symmetry with excitation energy increase, as well as the baryon spectrum narrowing owing to introduction of the quark-diquark states specifies a basic direction of investigations in this area. A separate problem arises due to the fact that predictions of quark models [3,7] and spectra of lattice QCD [1] are missing the parity doublet [$\Delta(1920)3/2^+$, $\Delta(1940)3/2^-$] that plays a key role in $\pi^0\eta$ photoproduction.

Predictions of these and also hybrid quark theoretical models [8] demonstrate the need to look for and clarify the coupling with the low-lying excitation modes for just those resonances whose amount for baryons is sufficiently greater than that observed experimentally in the elastic πN scattering. And for meson resonances (formed due to $q\bar{q}$ states), vice versa, is sufficiently less (and this leads to the so-called problem of missing resonances [2,9]). Specifics of electromagnetic interaction indicate that just electromagnetic excitation turns out to be most suitable for experimental studies of hadronic resonances. So far, couplings of the excited nucleon states with multimeson decay modes along with the $p\bar{p}$ annihilation are of paramount importance if we want to solve the problem of missing resonances. However, photoproduction of lightest pairs of pseudoscalar neutral mesons in coherent processes on light nuclei is characterized by two more very important specifics that are missing in the quasifree photoproduction of charged mesons:

(i) Effect of nuclear medium on the elementary photoproduction operator;
(ii) Distortion of meson yield due to the strong meson-nucleus final-state interaction.

No systematic investigations of these specifics were pursued within the unified photoproduction model that considers pairs of pseudoscalar mesons on light nuclei. Instead, independent simulation of the $\gamma \to \pi^0\pi^0$ and $\gamma \to \pi^0\eta$ reactions via partial-wave channels coupled with a certain baryon resonance is gaining popularity due to newly appeared high-precision experimental data on the polarized total and differential cross sections [10–13]. This simulation becomes possible by applying a simple χ^2 minimization of disagreement in the experimental findings and the so-called total likelihood function for the $\pi^0\pi^0N$ or $\pi^0\eta N$ system taking account of the experimental energy-angular correlations for the specified phase space [12,14,15]. But this makes the model to strongly depend on experimental results and reduces transparency of the approach on the whole. The traditional isobar approach [16–19] also uses sets of the effective Lagrangians that describe electromagnetic excitation and cascade decays of baryon resonances whose final state leads to three-particle states $\pi^0\eta N$ and $\pi^0\pi^0N$. Despite the fact that both approaches are good in describing total cross sections, the structure of the $\gamma \to \pi^0\eta$ and $\gamma \to \pi^0\pi^0$ transition amplitudes proved to be different and this is quite obviously demonstrated by the three-particle I^c, I^s asymmetries and the two-particle Σ asymmetry of the beam [12,20]. A complete experiment could put the

*egorovphys@mail.ru

matter to rest but implementation of such an experiment is technically difficult. In coherent processes of the $\pi^0\eta$ and $\pi^0\pi^0$ photoproduction on light nuclei, the effect of the nuclear medium reveals itself both in the creation operator modification depending on the atomic number of the target nucleus, and also in nonresonance contributions that change the shape of the cross section being differential over the invariant meson mass [21,22] or increase the total cross section [23]. Strong nonresonance contributions observed in the $\gamma \to \pi^0\pi^0$, $\gamma \to \pi^0\eta$ processes occurring due to the final-state interaction will be taken into account by the unified $\pi^0\pi^0$ and $\pi^0\eta$ pair photoproduction model that can be applied not only to describe polarization observables in the quasifree photoproduction, but also to describe coherent photoproduction on light nuclei. This statement directly results from isotopic selectivity adherent to operators of $\pi^0\pi^0$ and $\pi^0\eta$ photoproduction on light nuclei. This isotopic selectivity presupposes that on nuclei with the zero isospin, the $\gamma \to \pi^0\pi^0$ transition is due to isoscalar photons and the $\gamma \to \pi^0\eta$ transition is due to isovector ones. In view of isotopic selectivity, the cross section of such coherent processes as $\gamma \to \pi^0\pi^0$ (very preliminary data from Ref. [24], data from Ref. [25]) and $\gamma \to \pi^0\eta$ (data from Ref. [26]) on deuteron is of the order of several dozens of nanobarns and this is comparable to contributions of triple meson formation (e.g., $\pi^0\pi^0\pi^0$ [27]). The role belonging to the triple meson formation with the follow-on absorption of one of these mesons by nucleons in the coherent $\gamma \to \pi^0\pi^0$, $\gamma \to \pi^0\eta$ processes is also not investigated. In addition, it is very interesting to use the unified model of coherent $\pi^0\pi^0$ and $\pi^0\eta$ photoproduction on light nuclei in order to estimate the effect of all most important mechanisms of the meson-nucleus final-state interaction without involving any primitive optical mechanics models. For the first time, an attempt is undertaken to develop a rather simple and unified isobar model of the coherent $\pi^0\pi^0$ and $\pi^0\eta$ photoproduction on light nuclei with a great number of intermediate baryon resonances. Resonance parameters were determined on the assumption of the best description of available experimental data on total cross sections of the $\gamma \to \pi^0\pi^0$, $\gamma \to \pi^0\eta$ processes on proton and deuteron in the region of photon energy up to $E_\gamma = 2$ GeV. Availability of certain data on the coherent $\pi^0\pi^0$ photoproduction on nuclei with the open $1p$ shell, as well as the prospective experiment on a number of p-shell nuclei inspired me to make first estimates of total cross sections of the $\gamma \to \pi^0\pi^0$, $\gamma \to \pi^0\eta$ processes on stable Li isotopes with the help of different nuclear models. The role of the most probable mechanisms of the meson-nucleus final-state interaction is also studied for Li nuclei.

II. COHERENT $\pi^0\pi^0$ AND $\pi^0\eta$ PHOTOPRODUCTION ON NUCLEUS

Consider the coherent electromagnetic processes of $\gamma \to \pi^0\pi^0$ and $\gamma \to \pi^0\eta$ on nuclei. In a concise form, these processes can be written down using the following endothermal reaction:

$$\gamma(\vec{k},\vec{\epsilon}_\lambda) + A(\vec{p}_i, E_A) \to \pi^0(\vec{q}_\pi, E_\pi) + s(\vec{q}_s, E_s) + A(\vec{p}_f, E'_A), \tag{1}$$

where the target-nucleus and the final nucleus are denoted by A and kinematic variables, including photon polarization $\vec{\epsilon}_\lambda$, are given in brackets. In this case, (1) has $s \in (\pi^0, \eta)$. The unpolarized cross section of processes as in (1) are expressed by the following formula:

$$\frac{d\sigma}{d\Omega_{p_f} d\Omega_{q^*} d\omega_{\pi s}} = (2\pi)^{-5}\frac{E_A E_{A'} q^* p_f}{8E_\gamma W^2}\frac{1}{2(2J_i+1)}\sum_{M_i M_f \lambda}\left|T^\lambda_{M_i M_f}\right|^2. \tag{2}$$

The total system energy is denoted by W and the relative momentum of mesons in their own center-of-mass system is denoted by $\vec{q}^*$. The total spin of the target nucleus is J_i and the sum in (2) is taken over projections of the total target-nucleus spin. Matrix elements $T^\lambda_{M_i M_f}$ (photon polarization index $\lambda = \pm 1$) are determined from the general formula for matrix elements of the $\gamma \to \pi s$ transition operator. In this general formula, spectroscopic multipliers explicitly extract the active nucleon and also the spectator-nucleon system. In the LS presentation, these matrix elements are written as follows:

$$T^\lambda_{M_i M_f} = \left\langle s'l't', L'S'T', L_f S_f T_f J_f\right|\hat{T}^\lambda_A\left|slt, LST, L_i S_i T_i J_i\right\rangle. \tag{3}$$

Here in (3), the lowercase letters (slt) correspond to quantum numbers (spin, orbital moment, and isospin, respectively) of the active nucleon and the uppercase letters ($L_{i/f}S_{i/f}T_{i/f}J_{i/f}$) correspond to quantum numbers of the target nucleus with the initial and final state thereof denoted by letters i/f. The concise expression for matrix elements (3) is given in Appendix. When the laboratory energy of the E_γ photon is vastly superior to the energy of nucleon coupling in the nucleus and momenta of arising particles (π, s) is notably greater compared to the mean momentum of coupled nucleons, then in order to find $T^\lambda_{M_i M_f}$ it is reasonable to use impulse approximation wherein the operator of photoproduction on nucleus $\hat{T}_{\gamma A}$ is expressed in terms of the coherent sum of operators of photoproduction on an individual nucleon $\hat{T}_{\gamma N}$

$$\hat{T}^\lambda_{\gamma A} = \sum_{i=1}^{A}\hat{T}^\lambda_{\gamma N}, \tag{4}$$

and the nucleon-spectator system state extracted with the help of quantum numbers (LST) remains unchanged.

The amplitude of photoproduction on nucleon is factorized in the following form:

$$T^\lambda_{\gamma N} = F_{\gamma N\to N^*(J,L)}G_{N^*(J,L)}F_{N^*(J,L)\to sM^*}G_{M^*}F_{M^*\to tN}, \tag{5}$$

which depicts a strong coupling of the $N^*(J,L)$ resonance with the $s \in (\pi^0, \eta)$ meson and the intermediate $M^* \in [\Delta(1232), S_{11}(1535)]$ resonance. Coupling of the intermediate M^* resonance with the $t \in (\eta, \pi^0)$ mesons and the N nucleon is forming the final state for the elementary photoproduction operator. More precisely, the $2\pi^0N$ and $\pi^0\eta N$ final states result from the decay of the intermediate quasi-two-body states, i.e., $\pi\Delta$, σN for $2\pi^0N$ and $\eta\Delta$, $\pi S_{11}(1535)$, as well as a_0N for $\pi^0\eta N$, respectively.

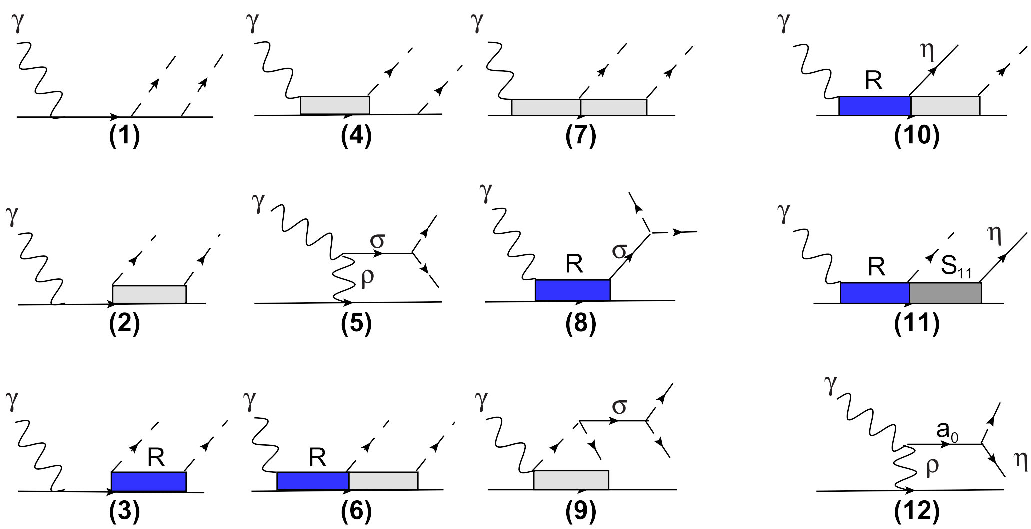

FIG. 1. Diagrams 1–9: $2\pi^0$ photoproduction model. Diagrams 10–12: $\pi^0\eta$ photoproduction model. Resonant contribution is shown in blue, $\Delta(1232)$ isobar is denoted by gray rectangular boxes.

Expressions for the electromagnetic $F_{\gamma N\to N^*(J,L)}$ and hadronic $F_{N^*(J,L)\to sM^*}, F_{M^*\to tN}$ vertex functions are derived using the nonrelativistic isobar model [17] with Born (diagrams 1, 2, 4, 5, 7, 9, 12 in Fig. 1) and resonant (diagrams 3, 6, 8, 10, 11 in Fig. 1) contributions calculated in the tree-level approximation. In my work, this model is expanded to have the $\pi^0\eta$ channel through inclusion of additional resonances, i.e., $N(1710)\frac{1}{2}^+$, $N(1880)\frac{1}{2}^+$, $N(1900)\frac{3}{2}^+$, $N(2100)\frac{1}{2}^+$, $\Delta(1750)\frac{1}{2}^+$, $\Delta(1900)\frac{1}{2}^-$, $\Delta(1905)\frac{5}{2}^+$, $\Delta(1920)\frac{3}{2}^+$, $\Delta(1940)\frac{3}{2}^-$. This expanded isobar model for the $N(\gamma,\pi^0\pi^0)N$ and $N(\gamma,\pi^0\eta)N$ processes includes just those resonances that fall within the photon energy region $E_\gamma < 2$ GeV and are marked with three and four asterisks in the Particle Data Group (PDG) compilation [28]. Propagators of baryon resonance $G_{N*(J,L)}$ and G_M were taken to have a simple Breit-Wigner form that guarantees correct behavior of the resonance only in the vicinity of its maximum value. Vertex functions $F_{\gamma N\to N^*(J,L)}$, $F_{N^*(J,L)\to sM^*}$, and $F_{M^*\to tN}$ were multiplied by the dipole attenuation factors with cutoff parameters Λ from Ref. [29]. For the electromagnetic $\gamma\to\pi^0\eta$ process, the background-Born terms of the amplitude $T_{\gamma N}$ are negligible and, therefore, it is sufficient to take into account only resonant contributions (diagrams 10–12 in Fig. 1). In addition to the widths of intermediate $\pi\Delta$ and σN states from [17], by analogy, I calculate partial widths of the intermediate $\eta\Delta$ states

$$\Gamma^{\eta\Delta}_{N^*(J,L)\to\pi^0\eta N} = \frac{1}{2\pi W}\sum_{\substack{l=|J-\frac{3}{2}|\\ l=\mathrm{mod}(2)}}^{J+\frac{3}{2}}\left(\frac{f^{(l)}_{\eta\Delta N^*}}{m^l_\pi}\right)^2\frac{l!M_\Delta}{(2l+1)!!}\int_{m_\pi+M_N}^{W-m_\eta}\frac{\omega_{\pi N}Q^{2l+1}}{2\pi M_\Delta}\left|G_\Delta(\omega_{\pi N})\right|^2\Gamma_\Delta(\omega_{\pi N})\,d\omega_{\pi N} \tag{6}$$

and also intermediate $\pi S_{11}(1535)$ states

$$\Gamma^{\pi^0 S_{11}}_{N^*(J,L)\to\pi^0\eta N} = \frac{1}{2\pi W}\sum_{\substack{l=|J-\frac{1}{2}|\\ l=\mathrm{mod}(2)}}^{J+\frac{1}{2}}\left(\frac{f^{(l)}_{\pi S_{11}N^*}}{m^l_\eta}\right)^2\frac{l!\,M_{S_{11}}}{(2l+1)!!}\int_{m_\eta+M_N}^{W-m_\pi}\frac{\omega_{\eta N}P^{2l+1}}{2\pi M_{S_{11}}}\left|G_{S_{11}}(\omega_{\eta N})\right|^2\Gamma_{S_{11}}(\omega_{\eta N})\,d\omega_{\eta N}, \tag{7}$$

coupled with the $\pi^0\eta$ channel. Masses of π^0, η mesons, the $\Delta(1232)$ and $N(1535)\frac{1}{2}^-$ resonances are denoted by m_π, m_η, M_Δ, and $M_{S_{11}}$, respectively. Momenta in vortices of the quasi-two-body decays Q and P are determined using the

TABLE I. Hadronic and electromagnetic coupling constants, as well as baryon resonant masses used in calculations. Superscript above the hadronic coupling constants indicates the orbital-wave state of the resonance in the specified channel.

N^*J^P	M (MeV)	g^M/g^E or $\{k_s,\ k_v\}_{E,M}$	$f^{(L)}_{\pi NN^*}$	$f^{(L)}_{\pi\Delta N^*}$	$f^{(L)}_{\eta\Delta N^*}$	$f^{(L)}_{\sigma NN^*}$	$f^{(L)}_{\pi S_{11}N^*}$
N(1440)$\frac{1}{2}^+$	1430	$\{0.072, 0.36\}_M, \{0, 0\}_E$	1.53^p	2.85^p	–	3.22^s	–
N(1520)$\frac{3}{2}^-$	1515	$\{0.55, 0.77\}_M, \{-0.01, 0.21\}_E$	0.3^d	$0.86^s/0.58^d$	–	–	–
N(1535)$\frac{1}{2}^-$	1547	$\{0, 0\}_M, \{-0.09, -0.27\}_E$	1.48^s	0.85^s	–	–	–
N(1650)$\frac{1}{2}^-$	1645	$\{0, 0\}_M, \{0.006, -0.12\}_E$	1.33^s	0.45^s	–	–	–
N(1675)$\frac{5}{2}^-$	1675	$\{-0.3, 0.6\}_M, \{-0.024, -0.023\}_E$	0.171^d	$0.57^d/0.05^g$	–	–	–
N(1680)$\frac{5}{2}^+$	1680	$\{0.2, 1.47\}_M, \{0.08, 0.25\}_E$	0.07^f	$0.33^p/0.076^f$	–	–	–
N(1700)$\frac{3}{2}^-$	1725	$\{-0.46, -0.54\}_M, \{-0.02, 0, 023\}_E$	0.123^d	$1.12^s/0.124^d$	–	–	–
N(1710)$\frac{1}{2}^+$	1710	$\{0, -0.24\}_M, \{0, 0\}_E$	0.21^p	0.54^p	1^p	2.21^s	1^p
N(1720)$\frac{3}{2}^+$	1720	$\{-0.06, -0.03\}_M, \{-0.025, 0.02\}_E$	0.27^p	1.28^p	–	–	–
N(1875)$\frac{3}{2}^-$	1875	$\{0.1, 0.1\}_M, \{-0.02, 0.03\}_E$	0.06^d	$1.59^s/0.2^d$	–	–	–
N(1880)$\frac{1}{2}^+$	1880	$\{0, 0\}_E, \{0.107, -0.22\}_M$	–	–	6.1^p	–	1^p
N(1900)$\frac{3}{2}^+$	1920	$\{-0.145, -0.016\}_M, \{0, 0\}_E$	–	–	0.84^p	–	1^p
N(2100)$\frac{1}{2}^+$	2100	$\{6.1, -0.125\}_M, \{0, 0\}_E$	–	–	1.85^p	–	3.5^p
N(2120)$\frac{3}{2}^-$	2030	$\{-0.136, 0.144\}_M, \{0.32, 0.124\}_E$	–	–	$4.2^s/0^d$	–	3^s
Δ(1232)$\frac{3}{2}^+$	1232	$-1.845/-0.087$	2.08^p	2.15^p	–	–	–
Δ(1600)$\frac{3}{2}^+$	1600	$-0.24/0.13$	0.48^p	0.95^p	2.44^p	–	1^p
Δ(1620)$\frac{1}{2}^-$	1620	$0/-0.1$	0.83^s	0.74^d	–	–	–
Δ(1700)$\frac{3}{2}^-$	1722	$0.1/-0.2$	0.13^d	$1.52^s/0.29^d$	5^s	–	5^s
Δ(1750)$\frac{1}{2}^+$	1832	$-0.26/-0.5$	–	–	4.8^p	–	0.54^p
Δ(1900)$\frac{1}{2}^-$	1860	$-0.25/-0.19$	–	–	3.6^d	–	1^s
Δ(1905)$\frac{5}{2}^+$	1880	$-0.72/-0.013$	0.016^f	$0.6^p/0.03^f$	$10^p/20^f$	–	1^p
Δ(1910)$\frac{1}{2}^+$	1910	$-0.11/0$	0.36^p	0.89^p	–	0^s	–
Δ(1920)$\frac{3}{2}^+$	1870	$-0.14/-0.73$	–	–	3^p	–	8^p
Δ(1940)$\frac{3}{2}^-$	1875	$-0.6/0.4$	0.13^d	$1.52^s/0.29^d$	$4.2^s/0^d$	–	3.5^s
Δ(1950)$\frac{7}{2}^-$	1940	$-0.23/-0.97$	0.005^g	$0.21^d/0.008^g$	–	–	–

triangular functions[1] λ

$$Q = \frac{\sqrt{\lambda(W, \omega_{\pi N}, m_\eta)}}{2W},$$
$$P = \frac{\sqrt{\lambda(W, \omega_{\eta N}, m_\pi)}}{2W}. \tag{8}$$

where $W, \omega_{\pi N}, \omega_{\eta N}$ is the total system energy and invariant masses of the meson-nucleon subsystems in formulas (6, 7, 8). Coupling of the Breit-Wigner propagators $G_{S_{11}}, G_\Delta$ and the resonant energy-dependent widths $\Gamma_{S_{11}}, \Gamma_\Delta$ is given by the following expressions:

$$G_\Delta(\omega_{\pi N}) = \left(\omega_{\pi N} - M_\Delta + \frac{i}{2}\Gamma_\Delta\right)^{-1},$$
$$\Gamma_\Delta = \frac{M_N}{2\pi W}\left(\frac{f^{(1)}_{\pi NN^*}}{m_\pi}\right)\frac{1}{3}\left(\frac{\sqrt{\lambda(\omega_{\pi N}, M_N, m_\pi)}}{2\omega_{\pi N}}\right)^3,$$

$$G_{S_{11}}(\omega_{\eta N}) = \left(\omega_{\eta N} - M_{S_{11}} + \frac{i}{2}\Gamma_{S_{11}}\right)^{-1},$$
$$\Gamma_{S_{11}} = \frac{M_N}{2\pi W} f^{(0)}_{\pi NN^*}\left(\frac{\sqrt{\lambda(\omega_{\eta N}, M_N, m_\eta)}}{2\omega_{\eta N}}\right). \tag{9}$$

In round brackets, the orbital moment that corresponds to a given resonance is shown over constants $f^{(l)}$. If I use PDG data to specify the total resonance width as Γ, then varying the fraction $\delta\Gamma/\Gamma$ of the total width as $\delta\Gamma/\Gamma = \Gamma^{\pi^0 S_{11}}_{N^*(J,L)\to\pi^0\eta N}$ and $\delta\Gamma/\Gamma = \Gamma^{\eta\Delta}_{N^*(J,L)\to\pi^0\eta N}$, I can find constants $f^{(l)}_{\pi S_{11}N^*}$ and $f^{(l)}_{\eta\Delta N^*}$ for each resonance N^*J^P, where J is its spin and $P = (-1)^l$ is its parity. So, all thus defined hadronic coupling constants are given in Table I. Masses of intermediate mesons (in MeV) were taken to be equal to $m_{a_0} = 980$, $m_\omega = 782$, $m_\rho = 770$, and $m_\sigma = 460$. The meson coupling constants were $f_{\gamma a_0\rho} \equiv f_{\gamma a_0\omega} = 4.2$, $f_{\sigma\pi\pi} = 3.59$, $f_{\gamma\sigma\rho} = 2.2$, $f_{\rho NN} = 3.07$, and $f_{a_0\pi\pi} = 1.77$. The coupling $N(1535)\frac{1}{2}^-$ with ηN is specified by the constant $f_{\eta NS_{11}} = 1.71$.

The electric g^E and magnetic g^M coupling constants for intermediate resonances with the isospin $T = 3/2$ were determined with the help of spiral amplitudes A_J for the resonance with the total spin $J = \frac{1}{2}, \frac{3}{2}$ and the orbital moment L following formulas $B13$–$B14$ from [17]. In case when resonance has

[1] $\lambda(\alpha, \beta, \gamma) = [(\alpha + \beta)^2 - \gamma^2][(\alpha - \beta)^2 - \gamma^2]$.

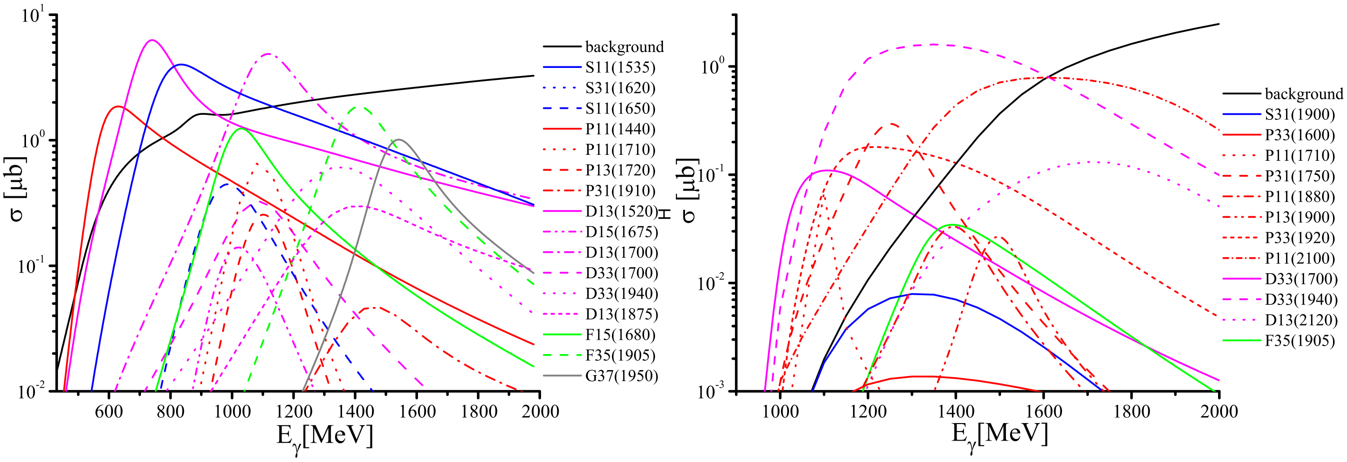

FIG. 2. Spectra of proton excitation into channels with $\pi^0\pi^0$ (left) and with $\pi^0\eta$ (right). Background and resonant contributions [designation in the format $L_{2T+2J}(M)$] are given as different colored lines.

isospin $T = 1/2$, spiral amplitudes $A^{(p/n)}_{\frac{1}{2}/\frac{3}{2}}$ are used to calculate constants for proton $g^{E/M}_{(p)}$ and for the neutron $g^{E/M}_{(n)}$. Equations for $g^{E/M}$ are used to find the isoscalar k_s and isovector k_v components of electromagnetic coupling constants according to formulas

$$k_s^{(E/M)} = \tfrac{1}{2}\big(g^{E/M}_{(p)} + g^{E/M}_{(n)}\big),$$
$$k_v^{(E/M)} = \tfrac{1}{2}\big(g^{E/M}_{(p)} - g^{E/M}_{(n)}\big). \tag{10}$$

With insufficient data on spiral amplitudes or partial widths of hadronic resonances in compilation from Ref. [28], calculations used the data of the nearest-in-mass resonances having the same parity. So, thus calculated isoscalar and isovector components of electromagnetic coupling constants are given in Table I. Figure 2 shows spectra given by the nonrelativistic isobar model for electromagnetic excitation of proton into channels with the $\pi^0\pi^0$ and $\pi^0\eta$ mesons.

III. FINAL-STATE INTERACTION OF π^0 AND η WITH NUCLEUS

Photoproduction of $\pi^0\pi^0$ and $\pi^0\eta$ pairs on nuclei has the following distinctive features:

(i) Absence of strong Born contributions such as the Δ-Kroll-Ruderman and meson pole contributions;
(ii) Great many hadronic resonances having a marked partial decay widths into channels with $\pi^0\pi^0$ and $\pi^0\eta$;
(iii) Strong dependence of the total cross section on the target nucleus isospin.

The first distinctive feature and the last one make us consider not only the main momentum mechanism of photoproduction, but also additional processes induced both by meson scattering from spectator nucleons, meson rescattering, and also by multiparticle processes of interaction in meson-nucleon sectors. It is also necessary to consider multimeson production with the follow-on complete absorption of some mesons by the target nucleus. The above contributions represent individual summands of the total amplitude of photoproduction on nucleus (3):

$$T_{M_iM_f} = T_{IA} + T_{MS} + T_{MMA} + T_{MBF}, \tag{11}$$

where T_{IA} are matrix elements of the photoproduction operator in the impulse approximation on nucleus and each summand of this operator in the sum (4) has contributions of diagrams in Fig. 1, i.e., T_{MS} is a summand that takes account of meson scattering on one or several spectator nucleons, T_{MMA} is the extended photoproduction operator that takes into account contributions from photoproduction of three and more mesons with the follow-on absorption of certain mesons by spectator nucleons, T_{MBF} is the contribution of many-body interaction of mesons with the final-state nucleus. In what follows, the photon polarization index λ will be omitted. The summand T_{MS} for the $\pi^0\pi^0$ channel is determined based on the well-parameterized separable $T_{\pi N}$ scattering amplitudes [30]. Mesons scattering in the $\pi^0\eta$ channel can be easily taken into consider if I take account of the following two facts:

(i) The $S_{11}(1535)$ resonance dominates in the ηN T matrix;
(ii) Probability of charged pion photoproduction in the vertex such as Δ-Kroll-Ruderman is almost one order of magnitude higher compared to neutral pion production probabilities.

In this context, the main contribution to mesons scattering in the $\pi^0\eta$ channel will come from processes 3, 4 in Fig. 3. The sum of contributions T_{MS} and T_{MMA} can be presented as an integral taken over the relative momentum of charge pion

$$\int \frac{d\vec{q}\,F(\Lambda, q^2)}{(2\pi)^3\omega_\pi(q)(\omega_\pi - \omega_\pi(q))}\big(\big(K_{N_1KR} + i\vec{\sigma}\vec{L}_{N_1KR}\big)\hat{\tau}_{KR}$$
$$\times\big(T_{sN_2}\hat{\tau}_{sN_2} + T_{N_2}\hat{\tau}_{N_2}\big) + \big(K_{R_1KR} + i\vec{\sigma}\vec{L}_{R_1KR}\big)\hat{\tau}_{R_2}\big)$$
$$+ (1 \Leftrightarrow 2). \tag{12}$$

Here indices $s = \pi^0$ and $R = \Delta$ for the $\gamma \to \pi^0\pi^0$ transition, as well as indices $s = \eta$ and $R = S_{11}(1535)$ for the $\gamma \to \pi^0\eta$ transition. The charged pion energy ω_π is specified on mass

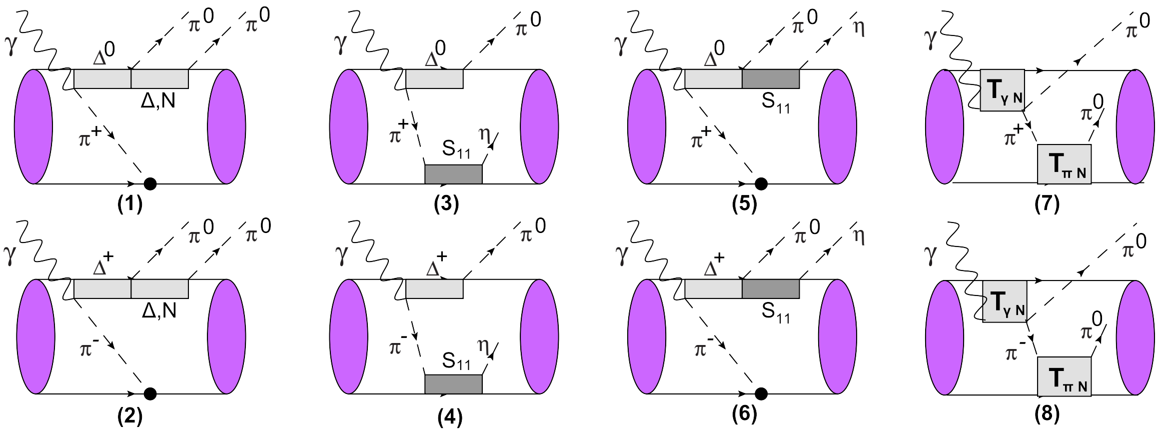

FIG. 3. Leading contributions to $\pi^{(+/-)}\pi^0\pi^0$ photoproduction (diagrams 1, 2) and $\pi^{(+/-)}\pi^0\eta$ photoproduction (diagrams 5, 6), as well as to the $\pi^{(+/-)}N \to \eta N$ rescattering (diagrams 3, 4) and $\pi^{(+/-)}N \to \pi^0 N$ rescattering (diagrams 7, 8). Ovals designate a pair of nucleons coupled in the nucleus.

shell. Indices 1 and 2 in (12) correspond to the injector nucleons and the acceptor nucleon, respectively. The hadron form factor $F(\Lambda, q^2)$ mimics the internal structure of the nucleon in strong meson-nucleon interaction and is found as the product of the standard dipole form factor by the cutoff function

$$F(\Lambda, q^2) = \frac{\Lambda^4}{\Lambda^4 + \left(\omega_{sN}^2 - M_\Delta^2\right)^2}\sqrt{1 - \exp\left(-\frac{10^6}{16Q_0^2}\right)}, \tag{13}$$

where Q_0 is the modulus of the sum when charged pion momenta are added to the active nucleon after photoproduction in the γN center-of-mass system. The relativized Δ-Kroll-Ruderman amplitude is determined from expressions

$$\begin{aligned} K_{N_1KR} + i\vec{\sigma}\vec{L}_{N_1KR} &= \alpha\left(\frac{f_{\pi N\Delta}}{m_\pi}\right)^2\sqrt{\frac{E_1 + M_N}{2M_N}}\sqrt{\frac{E_2 + M_\Delta}{2M_\Delta}}(K + i\vec{\sigma}\vec{L}) \\ K &= -\frac{2}{3}(\vec{q}_1\vec{\epsilon})\left(1 - \frac{\vec{p}\vec{k}}{(E_2 + M_\Delta)(E_1 + M_\Delta)}\right) - \frac{1}{3}[\vec{q}_1 \times \epsilon]\frac{[\vec{p} \times \vec{k}]}{(E_2 + M_\Delta)(E_1 + M_\Delta)} \\ \vec{L} &= \frac{2}{3}\vec{q}_1\vec{\epsilon}\frac{[\vec{p} \times \vec{k}]}{(E_2 + M_\Delta)(E_1 + M_\Delta)} - \frac{1}{3}[\vec{q}_1 \times \epsilon]\left(1 - \frac{\vec{p}\vec{k}}{(E_2 + M_\Delta)(E_1 + M_\Delta)}\right) - \frac{[\vec{q}_1 \times \epsilon][\vec{p} \times \vec{k}]}{3(E_2 + M_\Delta)(E_1 + M_\Delta)}, \end{aligned} \tag{14}$$

where $E_1, E_2, \vec{p}, \vec{k}$, and $\vec{q}_1$ is energy of the active nucleon, energy of the Δ isobar and its three-momentum, as well as the photon momentum and the momentum of a meson in the γN center-of-mass system, respectively. The amplitude of one pion absorption by the acceptor-nucleon T_{N_2} is determined according to a simple expression

$$T_{N_2} = -\left(\frac{f_{\pi NN}}{m_\pi}\right)^2\frac{\left(\vec{\sigma}^{[1]}_{\frac{1}{2}\frac{1}{2}}\vec{q}\right)\left(\vec{\sigma}^{[1]}_{\frac{1}{2}\frac{1}{2}}\vec{q}_2\right)}{\omega_{\pi N_2} - M_N}\frac{\Lambda_{\pi NN}^2}{\Lambda_{\pi NN}^2 + q^2}. \tag{15}$$

For transitions $\Delta \to \Delta$ from the Kroll-Ruderman vertex, the amplitude is given by the expression

$$K_{\Delta_1KR} + i\vec{\sigma}\vec{L}_{\Delta_1KR} = \alpha\left(\frac{f_{\pi N\Delta}}{m_\pi}\right)^2\frac{f_{\pi\Delta\Delta}}{m_\pi}\frac{f_{\pi NN}}{m_\pi}\frac{\left(\sigma^{[1]}_{\frac{1}{2}\frac{3}{2}}q_2^{[1]}\right)\left(\sigma^{[1]}_{\frac{3}{2}\frac{3}{2}}q_1^{[1]}\right)\left(\sigma^{[1]}_{\frac{3}{2}\frac{1}{2}}\epsilon^{[1]}\right)}{\left(\omega_{\pi N_2} - M_\Delta + i/2\,\Gamma_{\Delta_2}\right)\left(\omega_{\pi N_1} - M_\Delta + i/2\,\Gamma_{\Delta_1}\right)}. \tag{16}$$

For transitions $\Delta \to S_{11}(1535)$ from the Kroll-Ruderman vertex, the amplitude is given by the expression

$$\begin{aligned} K_{S_{11}KR} + i\vec{\sigma}\vec{L}_{S_{11}KR} = &-\left(K_{N_1KR} + i\vec{\sigma}\vec{L}_{N_1KR}\right)\frac{f_{\pi NN}}{m_\pi}\frac{f_{\pi S_{11}\Delta}}{m_\pi}\frac{f_{\eta NS_{11}}}{f_{\pi N\Delta}} \\ &\times\frac{\left(\sigma^{[1]}_{\frac{1}{2}\frac{1}{2}}q_2^{[1]}\right)\left(\sigma^{[1]}_{\frac{1}{2}\frac{1}{2}}q_1^{[1]}\right)}{\omega_{\eta N} - M_{S_{11}} + i/2\,\Gamma_{S_{11}}}\frac{\Lambda_{\eta NS_{11}}^4}{\Lambda_{\eta NS_{11}}^4 + \left(\omega_{\eta N_1}^2 - M_{S_{11}}^2\right)^2}. \end{aligned} \tag{17}$$

TABLE II. Matrix elements of operators τ that describe the isotopic structure of the coherent $\gamma \to \pi^+\pi^0\pi^0$ and $\gamma \to \pi^+\pi^0\eta$ processes.

$\gamma \to \pi^0 s$	τ_{KR}	τ_{sN_2}	τ_{N_2}	τ_R
$\gamma \to \pi^0\pi^0$	$\sqrt{\frac{2}{3}}$	$-\frac{\sqrt{2}}{3}$	$\frac{1}{\sqrt{3}}$	$\frac{2}{9\sqrt{5}}$
$\gamma \to \pi^0\eta$	$\frac{1}{3}$	$\sqrt{\frac{2}{3}}$	1	$-\frac{\sqrt{2}}{3\sqrt{3}}$

In Eqs. (14), (16), the fine structure constant is denoted by α and the spin operator matrices of rank $[r]$, which couple states with spins j_1 and j_2, are denoted by $\sigma^{[r]}_{j_1 j_2}$. The amplitude $T_{\eta N_2}$ entering the formula (12) for the $\gamma \to \pi^0\eta$ transition is easily determined from item (i) using the expression

$$T_{\eta N_2} = -\frac{f_{\eta N S_{11}} f_{\pi N S_{11}}}{\omega_{\eta N_2} - M_{S_{11}} + i/2\,\Gamma_{S_{11}}}. \tag{18}$$

For considered channels of mesons photoproduction, cutoff parameters for dipole form factors Λ were taken the same as in Ref. [29] but for appropriate indices of π and η that were changed where necessary. In the same work, I calculate the effect of the charged mesons rescattering into the neutral $\pi^+\pi^- \to 2\pi^0$ channel (diagram 9 in Fig. 1), and it has been shown that this effect may govern more than a half of the $\gamma \to \pi^0\pi^0$ cross section in region $E_\gamma < 500$ MeV.

In expression (12), isotopic operators $\hat{\tau}$ determine the isotopic structure of the$\pi^{+/-}\pi^0\pi^0$ and $\pi^{+/-}\pi^0\eta$ photoproduction on two nucleons. When the photoproduction operator affects the proton state, isotopic operators $\hat{\tau}$ have matrix elements given in Table II. As far as the Δ-Kroll-Ruderman term turns out to have the purely isovector isotopic structure, both transitions, i.e., $\gamma \to \pi^+\pi^0\pi^0$ and $\gamma \to \pi^+\pi^0\eta$, change their sign in the amplitude when π^+ changes to π^-, since

$$\langle p|\tau_{N_2}|n\rangle = -\langle n|\tau_{N_2}|p\rangle. \tag{19}$$

For this reason, the meson rescattering effects [Fig. 3] give only isovector contributions to the $\gamma \to \pi^0\pi^0$ and $\gamma \to \pi^0\eta$ transitions. It follows from condition (19) that on nuclei with the zero isospin, diagrams 7, 8 in Fig. 3 fail to give contribution to the cross section (i.e., isotopic selectivity).

Kinematics of all summands in formula (12) is determined by solving the following degenerate system of equations:

$$\begin{gathered}\vec{k} + \vec{p}_{1i} = \vec{q} + \vec{q}_1 + \vec{q}_2 + \vec{p}_{1f},\\ \vec{q}_{\rm in} = \tfrac{1}{2}(\vec{p}_{1i} - \vec{p}_{2i}), \quad \vec{q}\,'_{\rm out} = \tfrac{1}{2}(\vec{p}_{1f} - \vec{p}_{2f}),\\ \vec{p}_{1i} + \vec{p}_{2i} + \vec{k} = 0,\ \vec{p}_{1f} + \vec{p}_{2f} + \vec{q}_1 + \vec{q}_2\end{gathered} \tag{20}$$

with specified momenta $\vec{q}_{\rm in}, \vec{q}\,'_{\rm out}$, and $\vec{q}$. Momenta $\vec{p}_{1i}$, $\vec{p}_{2i}$ belong to the initial subsystem of nucleons and momenta $\vec{p}_{1f}$, $\vec{p}_{2f}$ to the final one. From the kinematic standpoint, transition from diagrams 1–2 and 5–6 to diagrams 3–4 in Fig. 2 reveals itself in the change of $\vec{q}$ to $\vec{q} - \vec{q}_2$.

The many-body mesons-nucleus interaction appears to be important particularly for the interaction of a slower η meson with the nucleus in the $\gamma \to \pi^0\eta$ process. It is most simple to take into account the three-body interaction in the subsystem ηd when the nucleon pair NN forms one coupled state having energy E_b, since above this energy, mesons scattering is accompanied by the opening of the inelastic deuteron-decay channel in the continuous energy spectrum. For heavier nuclei ^{3}He and ^{4}He, the three-body η-nuclear interaction is also important in the region of small kinetic energies of meson, though this interaction is not strong enough to form the coupled η-nuclear states [31]. Let us introduce a matrix potential

TABLE III. Parameters of two-body form factors ξ_i (25).

i	c_i (MeV)	b_i (fm^{-1})	$\lambda_{ii}, \lambda_{ij(j\neq i)}, \lambda_{ik(k\neq i,j)}$, (fm^{-1})		
π	-9×10^{-3}	42.3	-1,	8.6,	0.6
η	-1.1	2.7	8.6,	-1,	1.3
2π	5×10^{-2}	9.4	0.6,	1.3,	-1

$$V_{ij} = \begin{pmatrix} V_{\pi\pi} & V_{\pi\eta} & V_{\pi 2\pi} \\ V_{\eta\pi} & V_{\eta\eta} & V_{\eta 2\pi} \\ V_{2\pi\pi} & V_{2\pi\eta} & V_{2\pi 2\pi} \end{pmatrix}, \tag{21}$$

which acts on the state vector like $|\pi N, \eta N, 2\pi N\rangle$ only in the meson-nucleon sector. If potential (21) is parameterized in the separable form

$$V_{ij} = \xi_i \lambda_{ij} \xi_j, \tag{22}$$

wherein indices are running through the strictly determined sequence $i, j \in (\pi, \eta, 2\pi)$ and $\xi_{i/j}$ are the vertex form factors that are proportional to the impulse wave functions, then I have the exact solution of the two-body Lippmann-Schwinger equation Z_{ij} with potential (21). This exact solution Z_{ij} will be used in every meson-nucleon sector of the three-body problem of the η-NN nucleons interaction. The three-body π-NN interaction is found using the same solutions Z_{ij} (at $m_\pi \leftrightarrow m_\eta$) wherein the appropriate inelastic contributions are absent in the amplitude up to the η and $\pi\pi$ formation threshold energy. The procedure for solving the Faddeev three-body equations with two identical particles is well known and fully considered in my previous work [23]. I must solve the Faddeev equation for the three-body amplitude of the elastic scattering X_{dd} where index d belongs to the two-nucleon subsystem NN. After the three-body problem is solved, contribution of three-body forces to the general scattering matrix is determined through integration over the relative momentum of the meson η and the subsystem NN

$$T_{MBF} = \int T_{IA} \tau_{dd} X_{dd}, \tag{23}$$

where τ_{dd} is the two-body propagator of the subsystem NN operating in the phase space of the η-NN system. In expansion of Ref. [32] by the orbital moment for the elastic scattering matrix X_{dd}, I constrained myself only to two summands

$$X_{dd} = 4X^{[0]}_{dd} Y^2_{00}\big/\sqrt{2} - \left[Y^{[1]} \otimes Y^{[1]}\right]^{[0]} X^{[1]}_{dd}\big/\sqrt{2}. \tag{24}$$

Here, the orbital moment is given in square brackets and Y are spherical functions. Since the S_{11} resonance state that couples two channels, i.e., πN and ηN dominates in the η nucleon scattering, the orbital moment constraint is well founded. In contrast with [23], the two-body interactions are parametrized by the phase shift of the elastic πN scattering and by the total

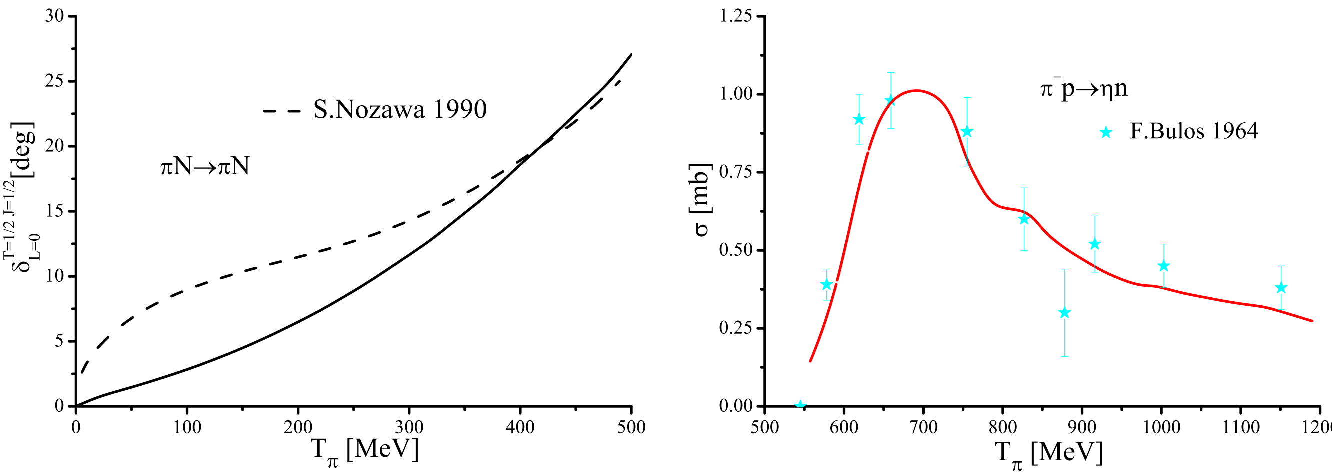

FIG. 4. Phase shift S_{11} of the elastic πN scattering (left) and cross section of the inelastic $\pi^- p \to \eta n$ scattering (right). Experimental points of the inelastic process [33]; data on the S_{11} phase shift [30].

cross section of the inelastic $\pi^- p \to \eta n$ scattering rather than by individual components of the matrix Z_{ij}. In this case, meson channels i are symmetric in the scattering matrix, since the potential is of the form given in (21). The two-body meson-nucleon form factors ξ_i are taken in the following form:

$$\xi_i = c_i \exp\left(-\frac{p^2}{b_i^2}\right). \qquad (25)$$

The relative momentum p is related to vertexes πN, ηN, and $2\pi N$. Values of parameters c_i, b_i, and λ_{ij} are given in Table III.

For the NN scattering, I use the more exact Bonn nucleon-nucleon potential of rank 4 [34] and, therefore, all form factors appear to have additional indices in accordance with their rank. However, all these indices are omitted for simplicity of mathematical notation. The scattering length $a_{\eta d}$ with the indicated NN potential was $-2.16 + i0.0415$ fm and this is close to the appropriate result from [31]. The calculated phase shift $\delta_{L=0}^{T=1/2,J=1/2}$ of the elastic πN scattering and the calculated total cross section of the inelastic $\pi^- p \to \eta n$ scattering are given in Fig. 4. As is obvious, my parametrization allows me to describe both the phase shift of the elastic s-wave scattering and also the inelastic scattering cross section. The other matrix components Z_{ij} that describe the inelastic $\pi \to 2\pi$ process, as well as the process inverse thereto are of no interest in this work. Therefore, they were found using only data described in Fig. 4.

IV. RESULTS

A. Proton

Spectra of the γ quantum-excited hadronic resonances contributing to the total cross section of the $p(\gamma, \pi^0\pi^0)p$ and $p(\gamma, \pi^0\eta)p$ reactions are given in Fig. 2. Compared to predictions from [15,17], resonance $D_{13}(1700)$ turns out to be the leading contributor to the cross section of the $\gamma \to \pi^0\pi^0$ process in the third resonance region at $E_\gamma \approx 1.2$ GeV. Contributions from resonances $D_{33}(1940)$, $P_{11}(1710)$, and $S_{11}(1650)$ are comparable and very small. In the region of the

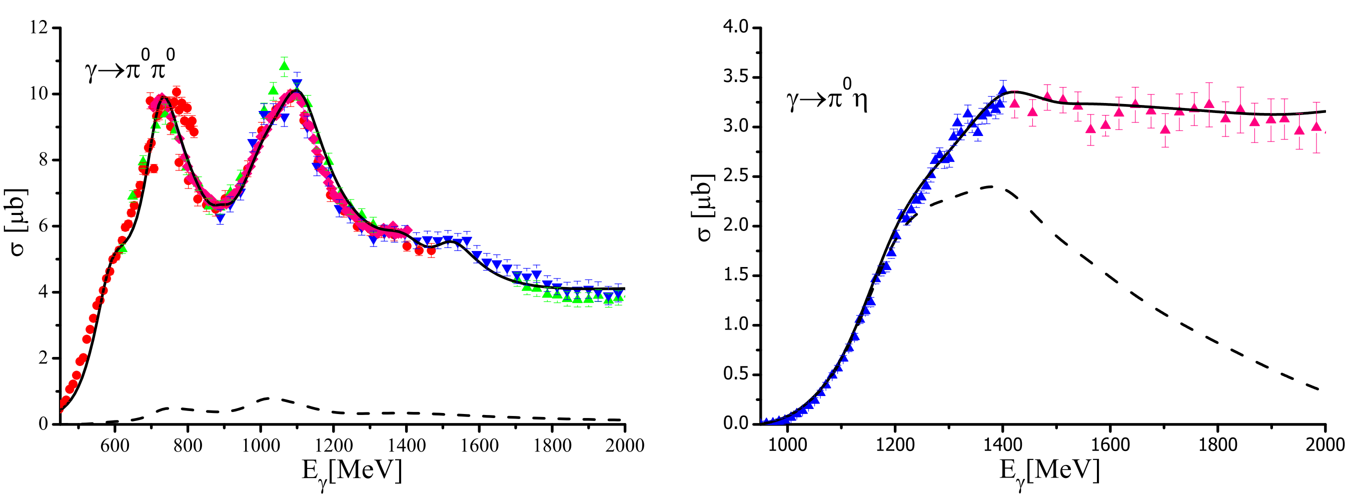

FIG. 5. Total cross section of $p(\gamma, 2\pi^0)p$ (left) and $p(\gamma, \pi^0\eta)p$ (right). Black solid lines show my predictions, dashed lines correspond to isoscalar contribution (left) and isovector contribution (right). Experiment $p(\gamma, 2\pi^0)p$: triangles [35], circles [36], diamonds [37]. Experiment $(\gamma, \pi^0\eta)p$: blue triangles [38], gray triangles [12].

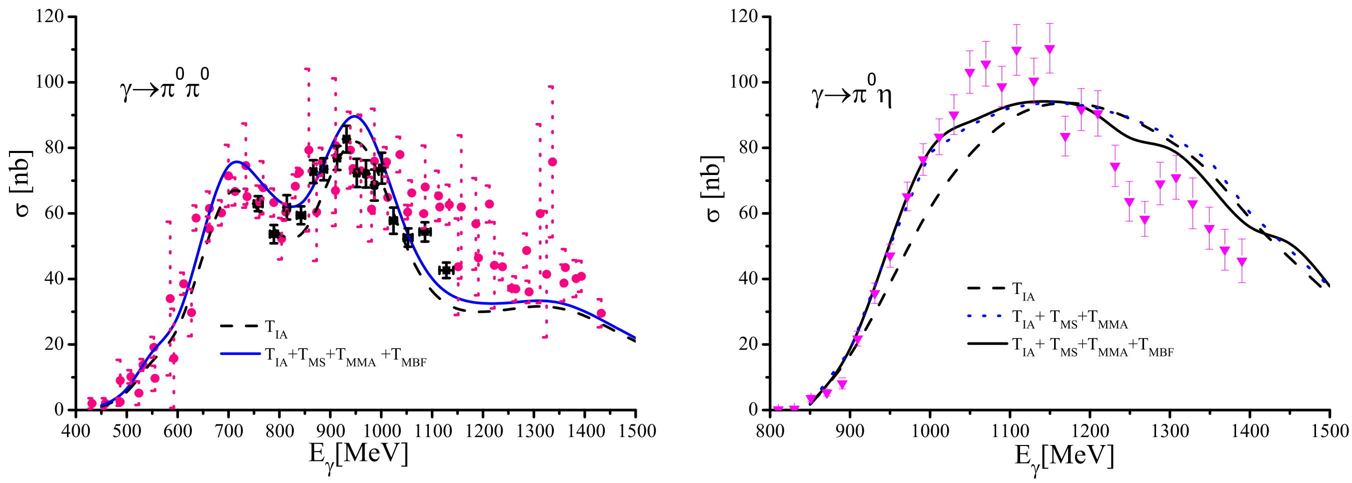

FIG. 6. Total cross section of $d(\gamma,\pi^0\pi^0)d$ (left) and $d(\gamma,\pi^0\eta)d$ (right). Very preliminary data for $d(\gamma,\pi^0\pi^0)d$: points [24], and squares [25]. Data for $d(\gamma,\pi^0\eta)d$ [26].

fourth resonance at $E_\gamma \approx 1.45$ GeV, resonances $F_{35}(1905)$ and $G_{37}(1950)$ appear to be rather influential. In my calculations, merely diagram 12 in Fig. 1 serves as the background for the $\gamma \rightarrow \pi^0\eta$ process. Contribution of diagram 12 to the cross section is completely ruled out due to the isoscalar nature of the $\gamma \rightarrow a_0(\rho - NN, \omega - NN) \rightarrow \pi^0\eta$ process taking account of isotopic selectivity observed to appear on the zero isospin nuclei, particularly on deuteron. In the energy region E_γ up to 2 GeV, the main hadronic resonances that are major contributors to the cross section are $D_{33}(1700)$, $P_{33}(1920)$, $P_{31}(1750)$, $D_{33}(1940)$, and $P_{11}(1880)$. Figure 5 presents the total cross section of the $p(\gamma,\pi^0\pi^0)p$ and $p(\gamma,\pi^0\eta)p$ processes. Dashed lines show contribution made by the isoscalar part of the amplitude for the $p(\gamma,\pi^0\pi^0)p$ process and the isovector part thereof for the $p(\gamma,\pi^0\eta)p$ process. As will be shown below, the form of both the isovector contribution to the $p(\gamma,\pi^0\eta)p$ cross section, and isoscalar contribution to the $p(\gamma,\pi^0\pi^0)p$ cross section is seen to agree with the recent results on total cross sections of processes $d(\gamma,\pi^0\eta)d$ [26] and $d(\gamma,\pi^0\pi^0)d$ [25], respectively. Notice that simple variation of spiral amplitudes A_J in a rather wide range of values for resonances from Table I (which contribute to the $\pi^0\eta$ channel) fails to give another relation between the isoscalar and isovector parts of the $\gamma \rightarrow \pi^0\eta$ process amplitude, which could give a correct description of total cross sections, i.e., $p(\gamma,\pi^0\eta)p$ and $d(\gamma,\pi^0\eta)d$.

B. Deuteron

As noted in Sec. I, due to absence of neutron targets I have to look for parameters of total amplitudes of $\gamma \rightarrow \pi^0\eta$ and $\gamma \rightarrow \pi^0\pi^0$ just relying upon the data on photoproduction on deuteron that acts as a filter towards isoscalar contributions to $\gamma \rightarrow \pi^0\eta$ and towards isovector contributions to $\gamma \rightarrow \pi^0\pi^0$. In the first approximation, processes that have the Δ-Kroll-Ruderman vertex (given in Fig. 3) are most important from among those responsible for the final-state interaction. Because of this vertex, exchange of charged pions in $NN \rightarrow NN$ will lead to the increase of the cross section rather than to its decrease. Figure 6 demonstrates just this growth for processes $d(\gamma,\pi^0\eta)d$ and $d(\gamma,\pi^0\pi^0)d$. Recall that due to its action, the deuteron filters out mechanisms 7–8 shown in Fig. 3. That is why, absorption of pions by spectator nucleons, what is common with the meson optics, is impossible in the case of the $d(\gamma,\pi^0\pi^0)d$ process. Good agreement between the impulse approximation for the total cross section of the $d(\gamma,\pi^0\pi^0)d$ process [17] and the data from [25] indirectly confirms this. The phenomenological wave function of deuteron was found based on the analysis of [39]. Phase shifts of NN scattering obtained based on this function are in agreement with experimental data right up to 500 MeV of the kinetic energy of one nucleon in laboratory frame.

TABLE IV. Quantum numbers for different target nuclei in calculations by formula (A2). Notation of grouped indices $i \in [0, 1]$, $t \in [0, 1, 2,]$, $p \in [0, 1, 2, 3]$, $h \in [0, 1, 2, 3, 4]$. One-body states are denoted by $[f]^{2T\,2S}l$ for the shell model. For ^{3}He, data are given for five channels [40].

State	lst	LST	$L_{i/f}\,S_{i/f}\,T_{i/f}$	$J_{i/f}$	$\bar{s}\,\bar{t}\,\bar{L}\,\bar{J}$
N	$0\ \frac{1}{2}\ \frac{1}{2}$		$0\ \frac{1}{2}\ \frac{1}{2}$	$\frac{1}{2}$	i i 0 i
d	(0,2) $\frac{1}{2}\ \frac{1}{2}$	(0,2) $\frac{1}{2}\ \frac{1}{2}$	(0,2) 1 0	1	i 0 t t
^{3}He$_{(N-D)}$	$0\ \frac{1}{2}\ \frac{1}{2}$	0 0 1	$0\ \frac{1}{2}\ \frac{1}{2}$	$\frac{1}{2}$	i i 0 i
	0	0 1 0	0	$\frac{1}{2}$	0
	2	0 1 0	2	$\frac{1}{2}$	h
	0	2 1 0	2	$\frac{1}{2}$	0
	2	2 1 0	h	$\frac{1}{2}$	h
$[4]^{11}S$	$0\ \frac{1}{2}\ \frac{1}{2}$	$0\ \frac{1}{2}\ \frac{1}{2}$	0 0 0	0	0 0 0 0
$[2]^{13}S$	$0\ \frac{1}{2}\ \frac{1}{2}$	$0\ \frac{3}{2}\ \frac{1}{2}$	0 1 0	1	i 0 0 i
$[3]^{22}P$	$1\ \frac{1}{2}\ \frac{1}{2}$	(0,2) i i	$1\ \frac{3}{2}\ \frac{1}{2}$	$\frac{3}{2}$	i i t p
^{6}Li$_{(d-\alpha)}$	(0,2) 1 0	0 0 0	0 1 0	1	i 0 0 i
	0 0 0	(0,2) 1 0	0 1 0	1	0 0 0 0
^{7}Li$_{(t-\alpha)}$	$0\ \frac{1}{2}\ \frac{1}{2}$	1 0 0	$1\ \frac{1}{2}\ \frac{1}{2}$	$\frac{3}{2}$	i i 0 i
	1 0 0	$0\ \frac{1}{2}\ \frac{1}{2}$	$1\ \frac{1}{2}\ \frac{1}{2}$	$\frac{3}{2}$	0 0 i i

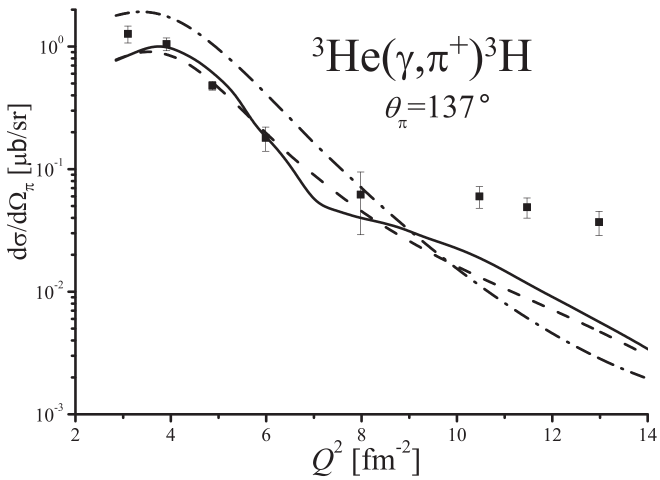

FIG. 7. Differential cross section $d\sigma/d\Omega_\pi$ at $\theta_\pi = 137^\circ$ for process $^3\mathrm{He}(\gamma,\pi^+)^3\mathrm{H}$ versus the squared transferred momentum Q^2. Elementary photoproduction operator is constructed based on the analysis of Ref. [18], dashed (solid) curve calculation in the impulse approximation (taking account of the mechanismlike diagram 1 in Fig. 3), dash-dotted line, calculation according to (27). Experimental data [41].

Accounting of the three-body π-NN and η-NN forces according to the model is shown in Fig. 6 as a solid line. Contributions of three-body forces turn out to be negligible for the $d(\gamma,\pi^0\pi^0)d$ process (the result merges with the calculation without these forces). At the same time, the η-NN interaction appears to be essential for the $d(\gamma,\pi^0\eta)d$ process not only in the region $E_\gamma < 1$ GeV [23], but also in the region $E_\gamma > 1.2$ GeV wherein the accounting of three-particle forces leads to the cross section decrease. This difference is attributed to specific features of the meson-nucleon interaction parametrization (21). As will be shown below, my assumed energy-independent intensity λ_{ij} of the meson-nucleon interactions fails to give sufficient growth of the η-NN interaction cross section in the η-meson region kinetic energy $T_\eta < 2.5$ MeV.

C. Helium-3

A very satisfactory parametrization of the wave function for the helium-3 nucleus is shown in Ref. [40]. Authors used both separable Paris and Bonn NN potentials to find the full $3N$ wave function of the three-nucleon system with the help of the Faddeev equations provided that the coupled (NN) part of the full wave function has eigen-normalization to unity. This wave function includes five independent partial-wave channels (quantum numbers of channels are also given in Table IV). In order to illustrate how successful is the parametrization of the three-nucleon ^{3}He wave function, Fig. 7 demonstrates calculation of the differential cross section $d\sigma/d\Omega_\pi$ relative to the polar π^+ meson escape angle $\theta_\pi = 137^\circ$ depending on the squared transferred momentum in the $^3\mathrm{He}(\gamma,\pi^+)^3\mathrm{H}$ reaction. Here, the dashed line is calculation in the impulse approximation with the use of the photoproduction operator constructed based on the partial-wave analysis of Ref. [18]. It is seen that up to $Q^2 = 8$ fm^{-2} (corresponds to the transferred momentum up to 550 MeV), calculation according to formula (A2) is in a nice agreement with the experiment. With the follow-on increase of the transferred energy, one observes that the so-called two-nucleon mechanisms of photoproduction begin to show up and contribution of one of these mechanisms, i.e., exchange of charged pions (analog of diagram 2 in Fig. 3 for the $\gamma \to \pi^+$ process), is given in Fig. 7 as the solid line. Calculation of total cross sections of processes $^3\mathrm{He}(\gamma,2\pi^0)^3\mathrm{He}$ and $^3\mathrm{He}(\gamma,\pi^0\eta)^3\mathrm{He}$ is given in Fig. 8. Compared to deuteron, helium-3 allows both isoscalar and isovector contributions to the $\gamma \to \pi^0\pi^0$ and $\gamma \to \pi^0\eta$ transitions. Nevertheless, cross sections of these processes turn out to be of the same order as similar cross sections of reactions with the deuteron target. As is shown below, this is due to specific features of the separable 3N wave function used in calculations. Contributions of processes from Fig. 3 prove to be essential in both cases: in the region between resonance peaks $800 < E_\gamma < 1100$ MeV for the $\gamma \to \pi^0\pi^0$ process and in the region $E_\gamma < 1300$ MeV for the $\gamma \to \pi^0\eta$ process only. Three-body forces were not taken into account for this nucleus and the next nuclei.

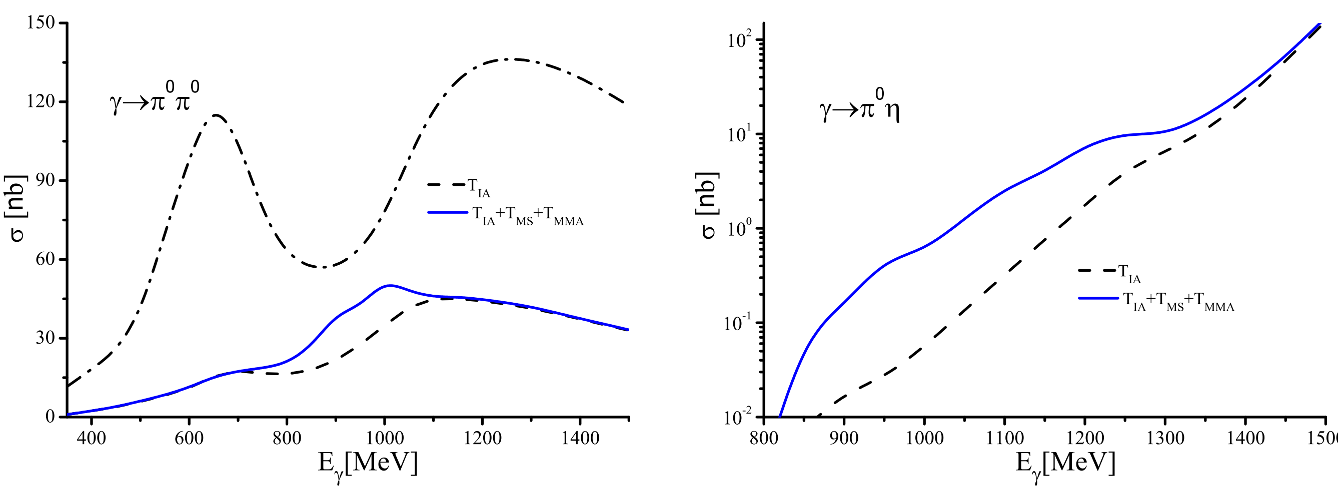

FIG. 8. Total cross section of $^3\mathrm{He}(\gamma,2\pi^0)^3\mathrm{He}$ (left) and $^3\mathrm{He}(\gamma,\pi^0\eta)^3\mathrm{He}$ (right). Dash-dotted line, calculation by (27).

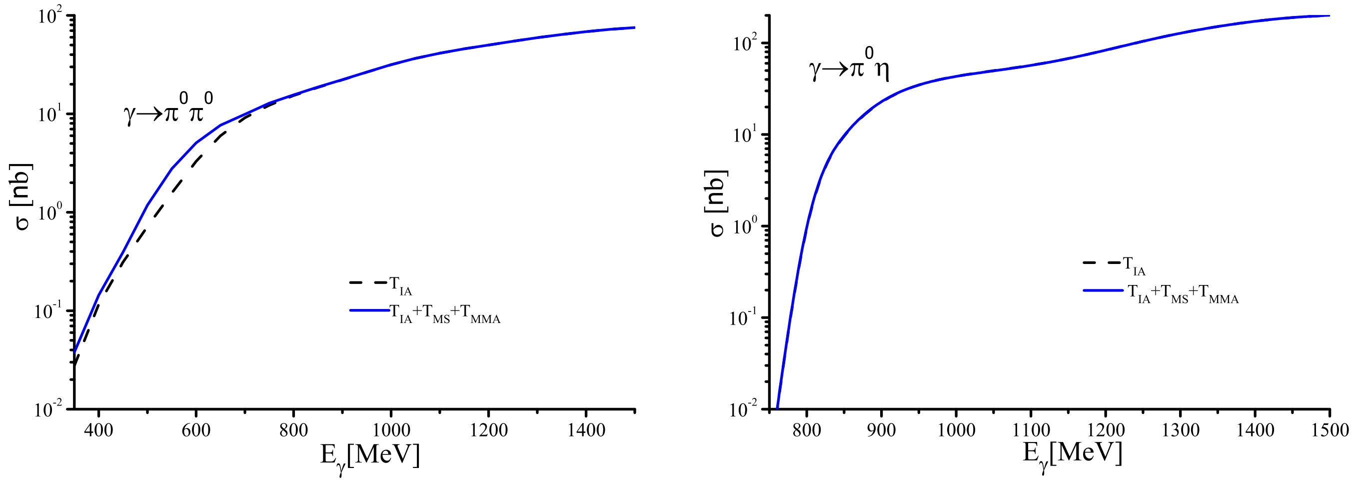

FIG. 9. Total cross section of ^{4}He$(\gamma, 2\pi^0)^4$He (left) and ^{4}He$(\gamma, \pi^0\eta)^4$He (right).

D. Helium-4

The helium-4 nucleus wave function parametrized based on distorted wave Born approximation (DWBA) with due consideration of exchange effects was derived in Ref. [42]. This function in coordinate representation has the following form:

$$\psi(r) = \frac{\exp(\alpha r)}{r} \sum_{j=1} a_j \exp(-\beta_j r). \tag{26}$$

In my calculations it is used the momentum distribution of ^{4}He nucleons, obtained with the help of the Fourier transform function (26) with the set of EXP1(MEC) parameters [42]. Accounting of exchange effects allows description of differential cross sections of proton scattering in the backward semisphere of angles in the region of high kinetic energies up to 800 MeV. Figure 9 shows calculations of cross sections of the ^{4}He$(\gamma, 2\pi^0)^4$He and ^{4}He$(\gamma, \pi^0\eta)^4$He processes with the given wave function. Accounting of rescattering and absorption of mesons by nucleon spectators (diagrams in Fig. 9) turns out to be important only in the $\gamma \to \pi^0\pi^0$ process in the region $E_\gamma = 500$–600 MeV.

E. Lithium-6, -7

Although microscopic wave functions are not available for these nuclei but merely usage of the shell-model wave function obtained based on the oscillatory potential can lead to a reasonable agreement with the experimental total cross section. Figure 10 demonstrates calculation of the total cross section of the ^{7}Li$(\gamma, \pi^0)^7$Li process compared to the data from Ref. [21]. The elementary photoproduction operator was found in pursuance of analysis in work [43] wherein the amplitude of $\gamma \to \pi^0$ was constructed taking account of the N, Δ Born terms and exchange of ω meson in the t channel. Angular configuration of the nuclear matrix element ^{7}Li$(\gamma, \pi^0)^7$Li was calculated by formula (A2) both for the shell wave functions purely from the Young tableau (solid line in Fig. 10), and also for the cluster functions formed by interaction of α particle and triton t (dashed line). Momentum distribution of cluster functions was taken the same as in the shell model with the parameter $p_0 = 2.9/\hbar c$ MeV^{-1}. Quantum numbers of wave functions are given in Table IV of Appendix. As it is seen from Fig. 10, just shell functions with the fitted oscillatory parameter p_0 give a fairly good agreement with the experimental data. Calculation of total cross sections of processes ^{6}Li$(\gamma, 2\pi^0)^6$Li, ^{7}Li$(\gamma, 2\pi^0)^7$Li and ^{6}Li$(\gamma, \pi^0\eta)^6$Li, ^{7}Li$(\gamma, \pi^0\eta)^7$Li with the shell-model wave functions having the oscillatory parameter p_0 is shown in Figs. 11 and 12. Contribution of diagrams from Fig. 3 is several dozens of nanobarns and it becomes notable for lithium nuclei only with the growth of energy $E_\gamma > 1200$ MeV.

V. DISCUSSION

The model of $\pi^0\pi^0$ and $\pi^0\eta$ photoproduction gives a rather good description of total cross sections of pairs production on proton. At the same time, differential cross sections that are more sensitive to model ingredients are rather worse reproduced. In Figs. 13 and 14 it is shown differential with respect to the meson invariant mass cross sections $d\sigma/d\omega_{\pi s}$. In the $\pi^0\pi^0$ channel, the distribution maximum is shifted towards smaller masses $\omega_{\pi\pi}$. Underestimation of the differential cross section in regions $E_\gamma = 520 \pm 20$ MeV and $E_\gamma = 720 \pm 20$ MeV testifies that either contribution of diagram 9 in Fig. 1 must be significant just in these regions, or, as shown in Ref. [29], hadronic coupling constants for $P_{11}(1440)$ and $D_{13}(1520)$ must be rather great in order to completely exclude contribution of rescattering $\pi^+\pi^- \to \pi^0\pi^0$ to the total cross section on proton. The differential cross section in the $\pi^0\eta$ channel is a good deal better reproduced in a wide region of photon energy $E_\gamma = 1050$–1450 MeV. Recent data on polarized cross sections of the $p(\gamma, \pi^0\eta)p$ process demonstrate that my model is in a rather good agreement with the experiment up to $E_\gamma = 1750$ MeV (Fig. 15). At higher energies, the value $\sigma_{1/2}$ begins to overestimate data and the value $\sigma_{3/2}$ to underestimate them. Despite certain disagreement between theoretical differential cross sections and experimental data for proton, my model of $\pi^0\pi^0$ and $\pi^0\eta$ photoproduction is quite suitable for investigation of

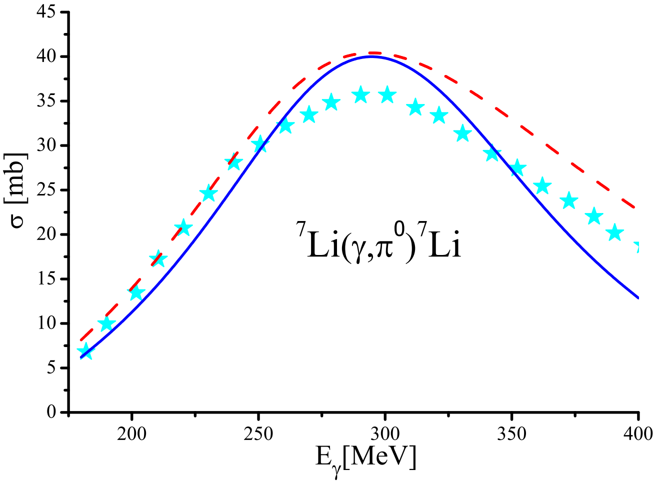

FIG. 10. Total cross section of $^7\mathrm{Li}(\gamma, \pi^0)^7\mathrm{Li}$, obtained using the shell model wave function of state $[3]^{22}P$ and using the angular structure of the $(\alpha - t)$ cluster configuration of ^{7}Li ground state with quantum numbers from Table IV. Experiment (stars) [21].

total cross sections on nuclei with atomic number $A \leqslant 7$, since it pretty exactly corresponds to experimental total cross sections on proton and deuteron. My direct calculations have demonstrated that mechanisms shown in Fig. 3 prove to be important for both channels, i.e., $\pi^0\pi^0$ and $\pi^0\eta$, in a wide region of photon energy. Recent experimental investigations [25] showed that deuteron escape in the backward semisphere of angles cannot be explained by such mechanisms as impulse approximation and this, according to that work, indicates appearance of isoscalar dibaryon states of deuteron with masses 2.38, 2.47, and 2.63 GeV. However, as it is clearly seen from Fig. 16 accounting of mechanisms from Fig. 3 increases cross section $d\sigma/d\Omega_d$ by an order of magnitude in the region $\cos(\theta_d) > -0.5$ at the total energy in the range $W_{\gamma d} = 2.7$–2.8 GeV. γ energy $E_\gamma \approx 1080$ MeV, when contribution of mechanisms shown in Fig. 3 is of the order of 10% of the total cross section, corresponds to this total energy. From this it follows that differential cross section $d\sigma/d\Omega_d$ of the $d(\gamma, 2\pi^0)d$ process in the region of the backward deuteron-escape angles $\cos(\theta_d) > -0.5$ can be explained with the help of mechanisms that are similar to those shown in Fig. 3 but make notably less than 10% contribution to the total cross section. These mechanisms also include production of a charged pion in the vertex like Δ-Kroll-Ruderman with the subsequent transitions $\Delta \to D_{33}$, $\Delta \to F_{35}$, etc., and charged pion absorption by the spectator nucleon. All these processes of $\pi^{+/-}\pi^0\pi^0$ production avoid the need to introduce the hypothetical dibaryon states of deuteron as it was done in Ref. [25] only with the purpose to explain the differential cross section $d\sigma/d\Omega_d$ in the region $\cos(\theta_d) > -0.5$. Note that due to low statistics, data from Ref. [25] are insufficient to unambiguously extract the quasifree $2\pi^0$ photoproduction peak in the region of small angles of deuteron escape and this obscures origin of experimental total cross section normalization. The three-body η-NN interaction, calculated using the Faddeev equation, with energy-independent intensities λ_{ij} of two-body interactions (21) also turns out to be important in the near-threshold region. Figure 17 shows the ratio of cross sections calculated with and without taking account of three-body forces. For the π-NN system wherein the inelastic η-N and 2π-N channels open only when the threshold energy is attained, one can see that these three-body forces are negligible and the cross-section ratio either with and without them is equal to unity. In regard to the η-NN system, accounting of the energy dependence λ_{ij} results in the characteristic growth of the cross section in the region of small η-meson kinetic energies (dash-dotted line in Fig. 17). When calculating cross sections on nuclei in my work, I restricted myself to accounting of three-particle forces only for deuteron and only for the case of energy-independent intensities. This calculation (see Fig. 8) demonstrates that even if accounting of the three-body interaction in the η-nuclear systems is important but the total cross section of $\pi^0\eta$ pairs photoproduction varies insignificantly compared to contributions of three-mesons production mechanisms (see Fig. 3) with the follow-on absorption of the charged meson and rescattering of charged pions from the spectator nucleon.

When passing to nuclei with $A > 2$, the wave function of the target nucleus becomes of key importance in describing cross sections of the coherent $\gamma \to \pi^0\pi^0$ and $\gamma \to \pi^0\eta$ pro-

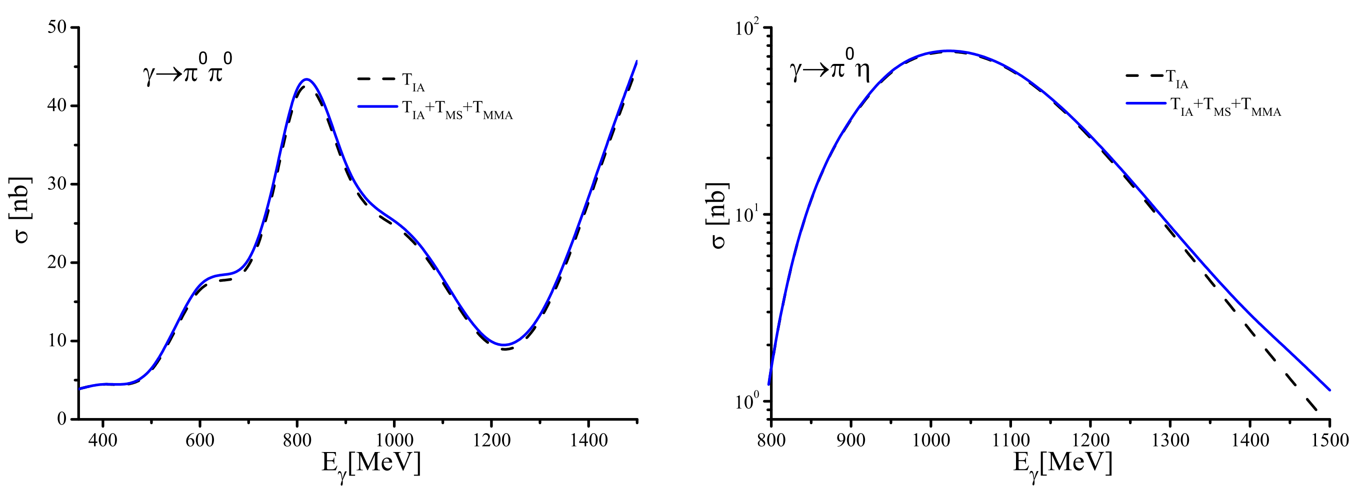

FIG. 11. Total cross section of $^6\mathrm{Li}(\gamma, 2\pi^0)^6\mathrm{Li}$ (left) and $^6\mathrm{Li}(\gamma, \pi^0\eta)^6\mathrm{Li}$ (right).

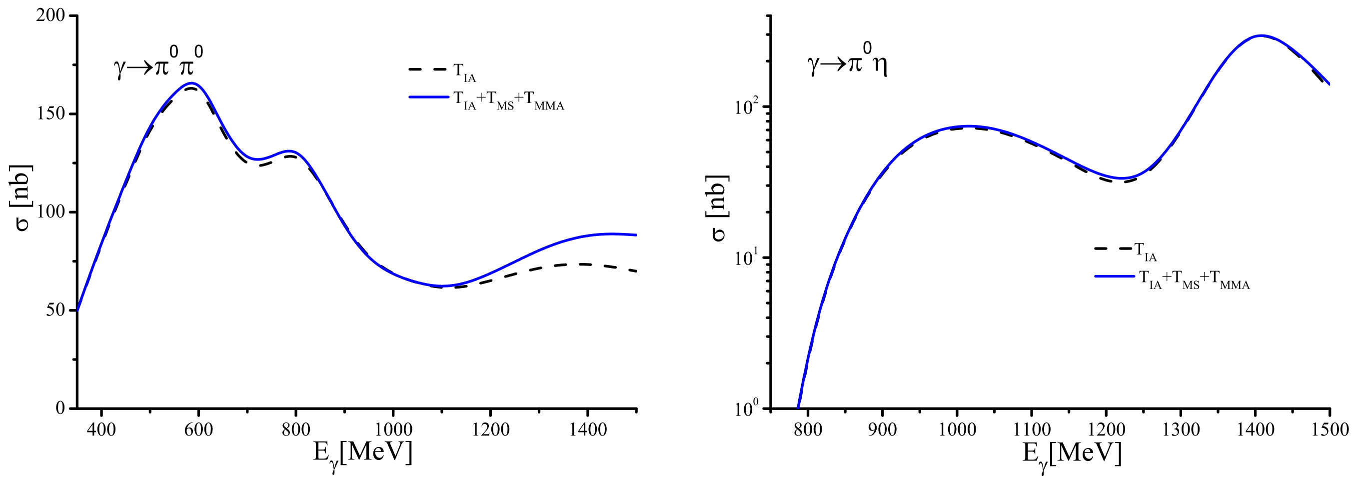

FIG. 12. Total cross section of ^{7}Li$(\gamma, 2\pi^0)^7$Li (left) and ^{7}Li$(\gamma, \pi^0\eta)^7$Li (right).

cesses. For ^{3}He, I use separable representation of the three-nucleon wave function found when three-body forces are precisely taken into consideration. Neglect of spectroscopic coupling between the active nucleon and the pair of spectator nucleons sufficiently changes the cross section. Amplitude of the $\gamma \to \pi\pi$ and $\gamma \to \pi\eta$ processes on ^{3}He nucleus in the impulse approximation without regard for the spectroscopic coupling between individual wave-function components can be written down as follows:

$$
\begin{aligned}
T^{\lambda}_{M_iM_f} &= \left\langle \left(j_1'\frac{1}{2}\right)\frac{1}{2}M_f \middle| K + \vec{L}\cdot\vec{\sigma} \middle| \left(j_1\frac{1}{2}\right)\frac{1}{2}M_f \right\rangle \\
&= \sum_\nu \delta_{j_1'j_1}\delta_{M_fM_i} \int \Psi^\nu(\vec{q}_{\rm in},\vec{q})\cdot K \cdot \Psi^\nu(\vec{q}_{\rm out},\vec{q}) \\
&\quad \times \frac{d^3q_{\rm in}d^3q}{(2\pi)^3} + \sum_\alpha \left\langle \left(j_1'\frac{1}{2}\right)\frac{1}{2}M_f \middle| \sigma^{[1]}_\alpha \middle| \left(j_1\frac{1}{2}\right)\frac{1}{2}M_i \right\rangle \\
&\quad \cdot (-1)^\alpha \int \Psi^\nu(\vec{q}_{\rm in},\vec{q}) L_{-\alpha} \Psi^\nu(\vec{q}_{\rm out},\vec{q}) \frac{d^3q_{\rm in}d^3q}{(2\pi)^3}.
\end{aligned}
\tag{27}
$$

K-spin free and $\vec{L}$-spin flip components of the photoproduction operator have an effect only on labels of the active nucleons $1/2M_i$ and $1/2M_f$ and as this takes place, I omit additional nucleus-related labels 1/2 in view of coincidence of ^{3}He nucleus spin and that of the nucleon. Relative momentum $\vec{q}$ is determined for the pair of spectator nucleons and it remains unchanged during photoproduction within the framework of impulse approximation, and as for momenta $\vec{q}_{\rm in}$ and $\vec{q}_{\rm out}$ determined for the active nucleon just prior to and after photoproduction. Summation with respect to ν in (27) is taken over numbers of channels independently of quantum numbers of one-particle components in the full wave function Ψ^ν for ^{3}He nucleus. Matrix element of the spin operator is determined using the following formulas of the angular momentum algebra:

$$
\begin{aligned}
&\left\langle (j_1'j_2')j'M_f \middle| \sigma^{[1]}_\alpha \middle| (j_1j_2)jM_i \right\rangle \\
&\quad = \sum_{b\beta} \delta_{j_1j_1'}(-1)^{j+j_1'+j_2-b}\sqrt{2j+1} \\
&\quad \times C^{j'M_f}_{jM_i\,b\beta} \begin{Bmatrix} j_1 & j_2 & j \\ j' & b & j_1' \end{Bmatrix} \langle j_1' || \sigma^{[b]} || j_1 \rangle.
\end{aligned}
\tag{28}
$$

In formula (28), the reduced matrix element $\langle j_1'||\sigma^{[b]}||j_1\rangle$ is equal to 1 at $b = 0$ and $\sqrt{6}$ at $b = 1$. In curly brackets of formula (28), one can see notation introduced for the Clebsch-Gordan coefficients $C^{j'M_f}_{jM_i\,b\beta}$ and for the $6j$ symbol. The dash-dotted line in Figs. 7 and 8 indicates cross sections calculated using the formula for amplitude (27). As we can see, neglect of the spectroscopic coupling between

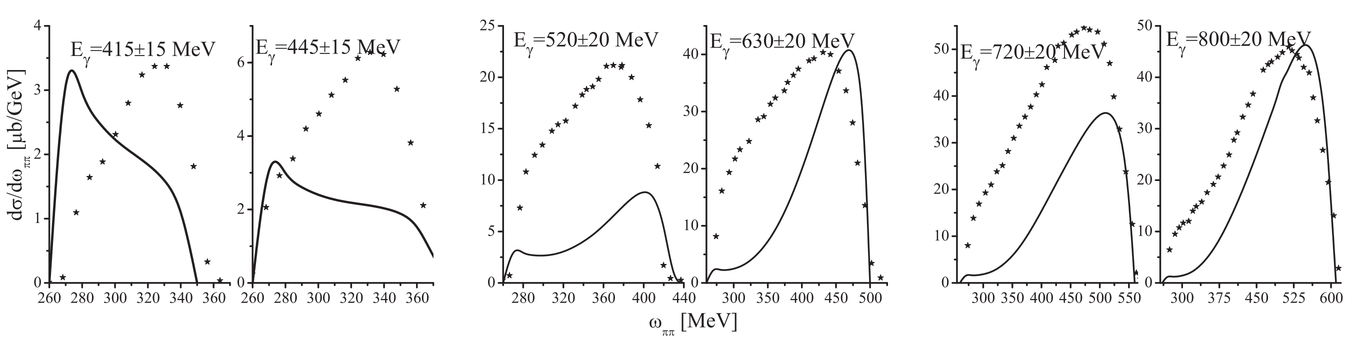

FIG. 13. Differential cross section $d\sigma/d\omega_{\pi\pi}$ of the $p(\gamma, \pi^0\pi^0)p$ process. γ-quantum energy is given in figures. Experiment [44].

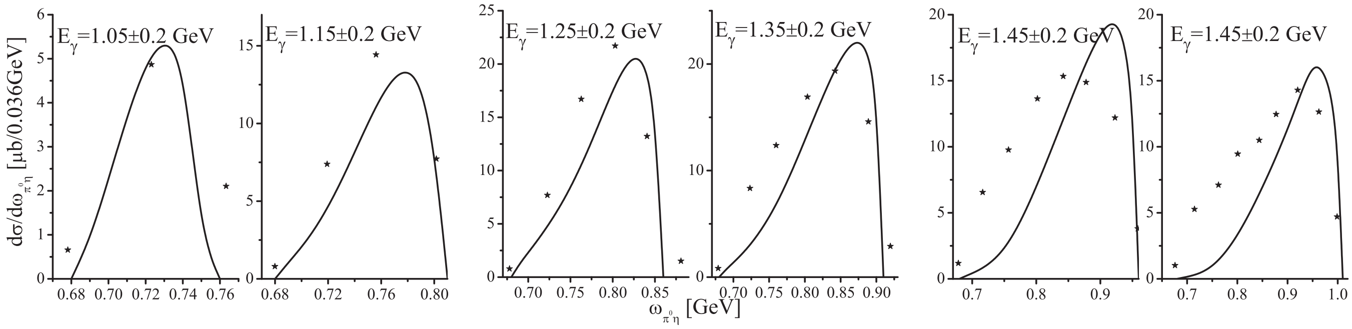

FIG. 14. Differential cross section $d\sigma/d\omega_{\pi^0\eta}$ of the $p(\gamma,\pi^0\eta)p$ process with arbitrarily normalized phase space. γ energy as 0.2 GeV class midmark is given in figures. Experiment [12].

individual components of the ^{3}He nucleus wave function seriously overestimates the $^3\mathrm{He}(\gamma,\pi^+)^3\mathrm{H}$ process cross section compared to experimental data, as well as the $^3\mathrm{He}(\gamma,\pi^0\pi^0)^3\mathrm{He}$ process cross section compared to a more exact calculation according to formula (A2).

The wave function of ^{4}He in parametrization [42] is insensitive to individual spin-angular states of the active nucleon and spectator nucleons. That is why we would expect that cross sections calculated using this wave function will be overestimated compared to the future experimental data.

For nuclei with $A > 4$, just the shell model with the intermediate LS coupling with the fitted oscillator parameter is likely to be sufficient in order to have good reproduction of the total cross section of the meson photoproduction processes. The total cross section of the $^7\mathrm{Li}(\gamma,\pi^0)^7\mathrm{Li}$ process (solid and dashed lines in Fig. 10) is known to vary slightly if I change only angular structure of the matrix element $T^{\lambda}_{M_iM_f}$, i.e., the p-shell structure is replaced by the cluster one (α-particle-triton). When calculating cross sections of the $\gamma \to \pi^0\pi^0$ and $\gamma \to \pi^0\eta$ processes on ^{6}Li and ^{7}L nuclei, the oscillatory parameter was taken equal to $2.9/\hbar c$. With the similar isotopic structure of the photoproduction operator, the total cross section of $^6\mathrm{Li}(\gamma,\pi^0\pi^0)^6\mathrm{Li}$ is not more than the $d(\gamma,\pi^0\pi^0)d$ cross section. Contribution of diagrams from Fig. 3 turns out to be negligible for the $\gamma \to \pi^0\pi^0$ transitions on nuclei with $A > 3$ and it is notable only in the region $E_\gamma \approx 1.5$ GeV. Of interest is the substantial influence of the nuclear wave function in $\gamma \to \pi^0\eta$ transitions. This influence makes itself evident in the fact that total cross sections of the $^4\mathrm{He}(\gamma,\pi^0\eta)^4\mathrm{He}$ and $^6\mathrm{Li}(\gamma,\pi^0\eta)^6\mathrm{Li}$ processes differ markedly though both nuclei have a zero isospin. Further advancement in the area of coherent double photoproduction of pseudoscalar mesons on nuclei with $A > 4$ can be due to newly appeared high-precision wave functions of these nuclei, which take into account both clusterization effects and also momenta imparted to spectator nucleons. Models of $A > 4$ nuclei, which take into account substantial momentum transferred to spectator nucleons, must be calibrated based on appropriate experimental data on light mesons photoproduction on these nuclei but these data are currently unavailable.

VI. CONCLUSION

This work is the first attempt to present the systematic approach that can be used to find cross sections for the coherent photoproduction of the $\pi^0\pi^0$ and $\pi^0\eta$ pairs on light nuclei. Elementary photoproduction operators were found using the isobar model having the intermediate baryon and meson resonances with hadron coupling constants that were selected on the assumption of better description of total cross

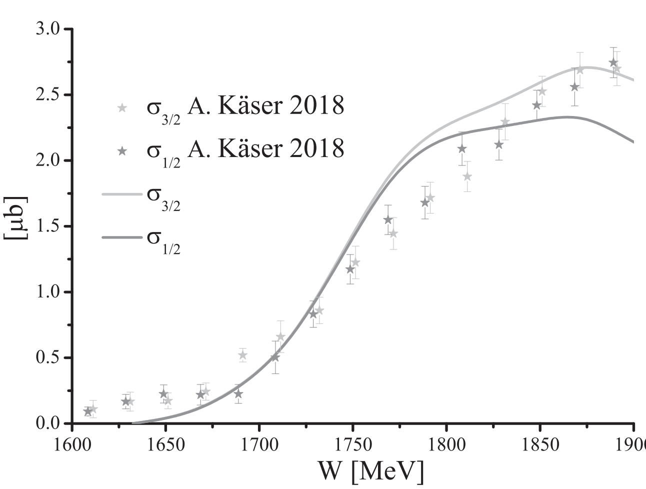

FIG. 15. Polarized cross sections $\sigma_{3/2}$ and $\sigma_{1/2}$ of the $p(\gamma,\pi^0\eta)p$ process versus total energy. Experiment [13].

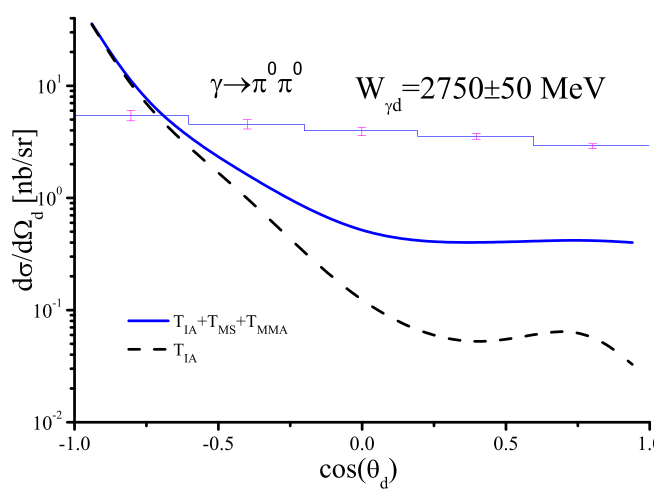

FIG. 16. Differential cross section $d\sigma/d\Omega_d$ of the $d(\gamma,2\pi^0)d$ process versus polar deuteron-escape angle θ_d. Total energy of the system is shown in the figure. Histogram is experiment [25].

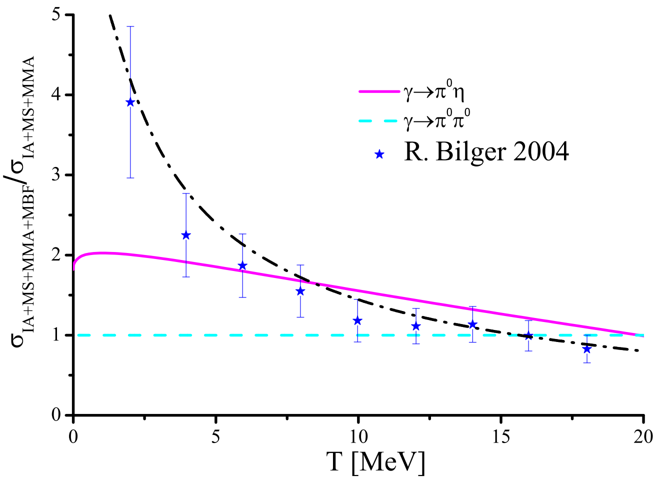

FIG. 17. Ratio of cross sections obtained with and without accounting of three-body forces versus meson kinetic energy T. Phase space is randomly normalized. Dash-dotted line is prediction from [23] with energy-dependent intensities λ_{ij}. Experiment for the $pd \to \eta pd$ [45].

sections for the $\gamma \to \pi^0\pi^0$ and $\gamma \to \pi^0\eta$ processes taking place on protons and deuterons. The work explicitly analyzes the meson-nucleus final-state interaction effects among which production of three mesons with the follow-on absorption of one of them by spectator nucleons was calculated for the first time. Calculated total cross sections of the $\gamma \to \pi^0\pi^0$ and $\gamma \to \pi^0\eta$ processes on nuclei with $A \leqslant 7$ demonstrate to be strongly dependent not only on the target nucleus isospin, but also on the selected model of the target nucleus.

At the end of this work I would like to point out that when the unified microscopic approach is used rather than poorly controlled optical models, the systematic study of electromagnetic $\gamma \to \pi^0\pi^0$ and $\gamma \to \pi^0\eta$ processes on light nuclei having different isospins gives most credible results compared to separate independent reinterpretations of one and the same data on the $\pi^0\pi^0$ and $\pi^0\eta$ photoproduction on light nuclei.

ACKNOWLEDGMENTS

Valuable discussion with Alexander Fix are much appreciated. The reported study was funded by RFBR, Project No. 20-02-00004.

APPENDIX

The nuclear wave function for the nucleus with A nucleons in the shell model with the intermediate LS coupling is written in the following form:

$$\Psi(\vec p_1, \vec p_2, \ldots, \vec p_A) = \sum_{lst}\sum_{LST}\sum_{m_l m_s m_t}\sum_{M_L M_S M_T} C^{S_i M_{S_i}}_{s m_s\, S M_S} C^{L_i M_{L_i}}_{l m_l\, L M_L} C^{T_i M_{T_i}}_{t m_t\, T M_T} \times U_{nl}(p_1) Y_{l m_l}(\hat p_1) \big|\xi_{s m_s}\big\rangle \big|\tau_{t m_t}\big\rangle \times \big(\alpha^{L_i S_i T_i; L_f S_f T_f}_{[f]LST}\, \beta_{[f]L_i S_i T_i; L_f S_f T_f}\big)^2 \times \Phi_{[f]L_i S_i T_i; L_f S_f T_f}(\vec p_2, \ldots, \vec p_A). \tag{A1}$$

One-body states are extracted from the nuclear wave function with the help of genealogical coefficients $\alpha^{L_iS_iT_i;L_fS_fT_f}_{[f]LST}$ and mixing $\beta_{[f]L_iS_iT_i;L_fS_fT_f}$ coefficients, both of which depend on the reduced Young scheme $[f]$ and quantum numbers, i.e., spin (S), orbital moment (L), and isospin (T) of the initial and final configurations of nucleus (i) and (f), respectively. When association probability for clusters with $A > 1$ in nucleus is close to unity, then in (A1) genealogy and mixing can be neglected if we take these multipliers to be ≈1. In (A1), multipliers C are the Clebsch-Gordan coefficients. Radial function of the active nucleon $U(p_1)$ is characterized by two quantum numbers nl of the nucleon subshell. The spin and isospin components of wave functions of the active nucleon are denoted by $|\xi_{sm_s}\rangle$ and $|\tau_{tm_t}\rangle$, respectively. Impulse approximation has the following characteristic feature. When energy of initiating particles is substantially higher than that of nucleons coupling in nucleus and the photoproduction operator is replaced by the sum of one-nucleon operators, the squared wave function of A-1 nucleons $\Phi_{[f]L_iS_iT_i;L_fS_fT_f}(\vec p_2, \ldots, \vec p_A)$, which enters matrix element (3) can be summed separately over quantum numbers of spectator nucleons that form the inactive subshell (cluster) with numbers (LST). As a result, the nuclear matrix element $T^{\lambda}_{M_f N_i}$ has the structure that is independent of spin parity and isospin of the intermediate baryon state. The occupation number for nucleons at the subshell (nl) and density of nucleons thereat are denoted by $N_{nls\to n'l's'}$ ($N_{nls\to n'l's'} = 4$ for the s shell) and $\rho_{nl}(p)$, respectively. In the cluster approach, density $\rho_{nl}(p)$ is replaced by density of cluster distribution in nucleus in the specified partial-wave state. Spherical functions $Y^{*[l']}[\hat p_1(p)]$ and $Y^{*[l]}[\hat p'_1(p)]$ depend on angle variables of the active nucleon (active cluster) prior to and after photoproduction. Accent $\hat x$ over the quantum number x is a shorthand notation for $\sqrt{2x+1}$.

As a result of extensive calculations that included multiple summation over magnetic quantum numbers of inactive nucleons within the framework of angular momentum algebra, this matrix element takes the following form:

$$T^{\lambda}_{M_f N_i} = \sum_{nlsn'l's'} N_{nls\to n'l's'} \sum_{\substack{L_iS_iT_i\\ L_fS_fT_f}} \int_0^\infty d^3p \sum_{\bar L\bar S\bar T}\sum_{[f]LST} \big(\alpha^{L_iS_iT_i;L_fS_fT_f}_{[f]LST}\, \beta_{[f]L_iS_iT_i;L_fS_fT_f}\big)^2 (-1)^{s+s'+l+l'+3S_i+L_i-J_i+\bar s-L-\bar L}(-1)^{-M_{J_f}+\bar m_t}$$
$$\times \hat T_i \hat t' \hat J_i \hat J_f \hat{\bar L} \hat S_f \hat L_f \hat L_i \hat S_i \hat s' C^{\bar J\bar M_J}_{J_iM_{J_i}\,J_f-M_{J_f}} C^{T_fM_{T_f}}_{T_iM_{T_i}\,\bar t-\bar m_t}\, i^{\bar s} \rho_{nl}(p) \begin{Bmatrix} \bar L & l' & l\\ L & L_i & L_f \end{Bmatrix} \begin{Bmatrix} s & S & S_i\\ S_f & \bar s & s' \end{Bmatrix} \begin{Bmatrix} t & T & T_i\\ T_f & \bar t & t' \end{Bmatrix} \begin{Bmatrix} S_f & L_f & J_f\\ S_i & L_i & J_i\\ \bar s & \bar L & \bar J \end{Bmatrix}$$
$$\times \Big[\big(K^{[\bar s][\bar t]}_{\lambda}\big)_{\bar m_t} \otimes \big[Y^{*[l']}(\hat p_1(p)) \otimes Y^{*[l]}(\hat p'_1(p))\big]^{[\bar L]}\Big]^{[\bar J]}_{\bar M_J}. \tag{A2}$$

In (A2), integration is done over the relative momentum of the active and inactive clusters (nucleons of the active and inactive subshell). Curly brackets include symbols $6j$ and $9j$. The line over the quantum number denotes quantum numbers imparted to nucleon of the (nl) subshell during the one-nucleon photoproduction. All quantum numbers involved in calculations are given in Table IV. Nucleonic state density $\rho_{nl}(p)$ calculated based on the normalized shell wave functions is determined as follows:

$$\rho_{00}(p) = \frac{4}{\sqrt{\pi}} p_0^3 \exp\left(-\frac{p_0^2}{2(p^2+p'^2)}\right),$$
$$\rho_{11}(p) = \frac{8p_0^5}{3\sqrt{\pi}} pp' \exp\left(-\frac{p_0^2}{2(p^2+p'^2)}\right). \tag{A3}$$

Relative momentum $\vec{p}$ of the active nucleon and also spectator nucleons of the target nucleus is specified as a variable whereas momentum $\vec{p}'$ has the meaning of the nucleon relative momentum after mesons photoproduction

$$\vec{p}' = \vec{p} + \vec{k} - \vec{q}_\pi - \vec{q}_s \tag{A4}$$

with momenta $\vec{q}_\pi, \vec{q}_s$. Photon momentum in (A4) $\vec{k}$. Parameter p_0 in (A3) was taken to be equal to $2.9/\hbar c$ MeV. Tensor components $(K_\lambda^{[\bar{s}][\bar{t}]})_{\bar{m}_t}$ are determined using spin-isospin components of the one-body photoproduction operator

$$\langle \xi_{s'm_{s'}} \tau_{t'm_{t'}} | T_{\gamma N} | \xi_{sm_s} \tau_{tm_t} \rangle$$
$$= \langle \xi_{s'm_{s'}} \tau_{t'm_{t'}} | K + \vec{K}\vec{\tau} + i(\vec{L} + \vec{\vec{L}}\vec{\tau})\vec{\sigma} | \xi_{sm_s} \tau_{tm_t} \rangle, \tag{A5}$$

where $K, \vec{K}$ are scalar-isoscalar and scalar-isovector components of the one-body operator and $\vec{L}$ and $\vec{\vec{L}}$ are pseudovector-isoscalar and pseudovector-isovector parts, respectively. The Wigner-Eckart theorem helps to couple components of the one-nucleon photoproduction operator with tensor operators in the following form: $K^{[0][0]} = K$, $K^{[0][1]} = \sqrt{3}\vec{K}$, $K^{[1][0]} = \sqrt{3}\vec{L}$, $K^{[1][1]} = 3\vec{\vec{L}}$. Formula (A2) also reflects that isotopic structures of $\gamma \to \pi^0\eta$ and $\gamma \to 2\pi^0$, processes are different and this difference makes itself evident in the fact that the isovector part of the amplitude for the $\gamma \to \pi^0\pi^0$ process and the isoscalar part thereof for the $\gamma \to \pi^0\eta$ process differ in sign on proton and neutron.

[1] R. G. Edwards, J. J. Dudek, D. G. Richards, and S. J. Wallace, Excited state baryon spectroscopy from lattice QCD, Phys. Rev. D **84**, 074508 (2011).

[2] S. Capstick and W. Roberts, Quasi-two-body decays of nonstrange baryons, Phys. Rev. D **49**, 4570 (1994).

[3] U. Löring, B. Metsch, and H. Petry, The light-baryon spectrum in a relativistic quark model with instanton-induced quark forces, Eur. Phys. J. A **10**, 395 (2001).

[4] E. Klempt and A. Zaitsev, Glueballs, hybrids, multiquarks: Experimental facts versus QCD inspired concepts, Phys. Rep. **454**, 1 (2007).

[5] D. Berenstein, C. P. Herzog, and I. R. Klebanov, Baryon spectra and ADS/CFT correspondence, J. High Energy Phys. 06 (2002) 047.

[6] H. Forkel and E. Klempt, Diquark correlations in baryon spectroscopy and holographic QCD, Phys. Lett. B **679**, 77 (2009).

[7] S. Capstick and N. Isgur, Baryons in a relativized quark model with chromodynamics, Phys. Rev. D **34**, 2809 (1986).

[8] J. J. Dudek and R. G. Edwards, Hybrid baryons in QCD, Phys. Rev. D **85**, 054016 (2012).

[9] E. J. Klempt and J. M. Richard, Baryon spectroscopy, Rev. Mod. Phys. **82**, 1095 (2010).

[10] V. Sokhoyan, Measurement of the polarization observables i^s and i^c in the reaction $\gamma p \to p\pi^0\pi^0$ with the CBELSA/TAPS experiment, AIP. Conf. Proc. **1432**, 405 (2012).

[11] V. Sokhoyan *et al.* (A2 Collaboration at MAMI), Experimental study of the $\gamma p \to \pi^0\eta p$ reaction with the A2 setup at the Mainz Microtron, Phys. Rev. C **97**, 055212 (2018).

[12] E. Gutz *et al.* (The CBELSA/TAPS Collaboration), High statistics study of the reaction $\gamma p \to p\pi^0\eta$, Eur. Phys. J. A **50**, 74 (2014).

[13] A. Käser *et al.*, First measurement of helicity-dependent cross sections in $\pi^0\eta$ photoproduction from quasi-free nucleons, Phys. Lett. B **786**, 305 (2018).

[14] U. Thoma *et al.* (The CBELSA/TAPS Collaboration), n^* and δ^* decays into $n\pi^0\pi^0$, Phys. Lett. B **659**, 87 (2008).

[15] A. Sarantsev *et al.* (CB-ELSA, and A.-T. Collaborations), New results on the roper resonance and the p_{11} partial wave, Phys. Lett. B **659**, 94 (2008).

[16] J. Gomez-Tejedor, M. Vicente-Vacas, and E. Oset, Double pion photoproduction in nuclei, Nucl. Phys. A **588**, 819 (1995).

[17] A. Fix and H. Arenhövel, Double-pion photoproduction on nucleon and deuteron, Eur. Phys. J. A **25**, 115 (2005).

[18] D. Drechsel, S. Kamalov, and L. Tiator, Unitary isobar model-maid2007, Eur. Phys. J. A **34**, 69 (2007).

[19] A. Fix, V. L. Kashevarov, A. Lee, and M. Ostrick, Isobar model analysis of $\pi^0\eta$ photoproduction on protons, Phys. Rev. C **82**, 035207 (2010).

[20] V. Sokhoyan *et al.* (A2 Collaboration at MAMI), Measurement of the beam-helicity asymmetry in photoproduction of $\pi^0\eta$ pairs on carbon, aluminum, and lead, Phys. Lett. B **802**, 135243 (2020).

[21] Y. Maghrbi, Photoproduction of mesons off ^{7}Li: Properties of hadron in nuclear matter, Ph.D. thesis, University of Basel, 2011.

[22] Y. Maghrbi *et al.*, Double pion photoproduction off nuclei - are there effects beyond final-state interaction?, Phys. Lett. B **722**, 69 (2013).

[23] M. Egorov and A. Fix, Coherent $\pi^0\eta$ photoproduction on $s-$shell nuclei, Phys. Rev. C **88**, 054611 (2013).

[24] I. Jaegle, 14th CB Meeting, Edinburgh, 2009 (unpublished).

[25] T. Ishikawa *et al.*, Non-strange dibaryons studied in the $\gamma d \to \pi^0\pi^0 d$ reaction, Phys. Lett. B **789**, 413 (2019).

[26] A. Käser *et al.*, The isospin structure of photoproduction of $\pi\eta$ pairs from the nucleon in the threshold region, Phys. Lett. B **748**, 244 (2015).

[27] A. Starostin *et al.*, Measurement of $3\pi 0$ photoproduction on the proton from threshold to 1.4 gev, arXiv:1101.3744.

[28] M. Tanabashi *et al.* (Particle Data Group), Review of particle physics, Phys. Rev. D **98**, 030001 (2018).

[29] R. Dusaev and M. Egorov, Double photoproduction of neutral pions on a proton and a deuteron, Russ. Phys. J. **60**, 26 (2017) [Izvestia Vuyzov. Phyzica **60**, 26 (2017)].
[30] S. Nozawa, A dynamical model of pion photoproduction on the nucleon, Nucl. Phys. A **513**, 459 (1990).
[31] A. Fix and O. Kolesnikov, Systematic few-body analysis of ηd, η^3He, and η^4He interaction at low energies, Phys. Rev. C **97**, 044001 (2018).
[32] M. Egorov, η^7Li scattering in the αt-cluster model, Phys. At. Nucl. **81**, 183 (2018).
[33] F. Bulos *et al.*, Total Cross Sections and Angular Distributions for $\pi^- + p \to \eta^0 + n$ from Threshold to 1151 MeV, Phys. Rev. Lett. **13**, 486 (1964).
[34] J. Haidenbauer, Y. Koike, and W. Plessas, Separable representation of the bonn nucleon-nucleon potential, Phys. Rev. C **33**, 439 (1986).
[35] V. Sokhoyan *et al.* (The CBELSA/TAPS Collaboration), High-statistics study of the reaction $\gamma p \to p2\pi^0$, Eur. Phys. J. A **51**, 95 (2015).
[36] Y. Assafiri *et al.*, Double π^0 Photoproduction on the Proton at Graal, Phys. Rev. Lett. **90**, 222001 (2003).
[37] V. Kashevarov *et al.* (Crystal Ball at MAMI, TAPS, and A. Collaborations), Experimental study of the $\gamma p \to \pi^0\pi^0 p$ reaction with the Crystal Ball/TAPS detector system at the Mainz Microtron, Phys. Rev. C **85**, 064610 (2012).
[38] V. Kashevarov *et al.* (Crystal Ball at MAMI, TAPS, and A. Collaborations), Photoproduction of $\pi^0\eta$ on protons and the $\delta(1700)d_{33}$-resonance, Eur. Phys. J. A **42**, 141 (2009).
[39] R. Machleit, K. Holinde, and C. Elster, The bonn meson-exchange model for the nucleon-nucleon interaction, Phys. Rep. **149**, 1 (1987).
[40] V. Baru, J. Haidenbauer, C. Hanhart, and J. Niskanen, New parametrization of the trinucleon wave function and its application to the π^3He scattering length, Eur. Phys. J. A **16**, 437 (2003).
[41] D. Bachelier, Pion photoproduction on ^{3}He at and above the 3-3 resonance, Phys. Lett. B **44**, 44 (1973).
[42] H. S. Sherif, M. S. Abdelmonem, and R. S. Sloboda, Exchange effects and large angle proton scattering on light nuclei at intermediate energies: Formalism and application to p+^{4}He scattering, Phys. Rev. C **27**, 2759 (1983).
[43] X. Li, L. E. Wright, and C. Bennhold, Exclusive quasifree pion photoproduction on complex nuclei in the δ region, Phys. Rev. C **48**, 816 (1993).
[44] Crystal Ball at MAMI, TAPS, and A. Collaborations, F. Zehr *et al.*, Photoproduction of $\pi^0\pi^0$-and $\pi^0\pi^+$-pairs off the proton from threshold to the second resonance region, Eur. Phys. J. A **48**, 98 (2012).
[45] R. Bilger *et al.*, Measurement of the $pd \to pd\eta$ cross section in complete kinematics, Phys. Rev. C **69**, 014003 (2004).